

Article

Development and Biological Evaluation of the First Highly Potent and Specific Benzamide-Based Radiotracer [¹⁸F]BA3 for Imaging of Histone Deacetylases 1 and 2 in Brain

Oliver Clauß ^{1,*}, Linda Schäker-Hübner ^{2,3}, Barbara Wenzel ¹, Magali Toussaint ¹,
Winnie Deuther-Conrad ¹, Daniel Gündel ¹, Rodrigo Teodoro ¹, Sladjana Dukić-Stefanović ¹,
Friedrich-Alexander Ludwig ¹, Klaus Kopka ^{1,4}, Peter Brust ¹, Finn K. Hansen ²
and Matthias Scheunemann ^{1,*}

- ¹ Department of Neuroradiopharmaceuticals, Institute of Radiopharmaceutical Cancer Research, Research Site Leipzig, Helmholtz-Zentrum Dresden-Rossendorf, 04318 Leipzig, Germany; b.wenzel@hzdr.de (B.W.); m.toussaint@hzdr.de (M.T.); w.deuther-conrad@hzdr.de (W.D.-C.); d.guendel@hzdr.de (D.G.); r.teodoro@life-mi.com (R.T.); s.dukic-stefanovic@hzdr.de (S.D.-S.); f.ludwig@hzdr.de (F.-A.L.); k.kopka@hzdr.de (K.K.); p.brust@hzdr.de (P.B.)
- ² Pharmaceutical and Cell Biological Chemistry, Pharmaceutical Institute, University of Bonn, 53121 Bonn, Germany; l.schaeker@uni-bonn.de (L.S.-H.); finn.hansen@uni-bonn.de (F.K.H.)
- ³ Institute for Drug Discovery, Medical Faculty, Leipzig University, 04103 Leipzig, Germany
- ⁴ Faculty of Chemistry and Food Chemistry, School of Science, Technical University Dresden, 01062 Dresden, Germany
- * Correspondence: o.clauss@hzdr.de (O.C.); m.scheunemann@hzdr.de (M.S.)



Citation: Clauß, O.;

Schäker-Hübner, L.; Wenzel, B.;

Toussaint, M.; Deuther-Conrad, W.;

Gündel, D.; Teodoro, R.;

Dukić-Stefanović, S.; Ludwig, F.-A.;

Kopka, K.; et al. Development and

Biological Evaluation of the First

Highly Potent and Specific

Benzamide-Based Radiotracer

[¹⁸F]BA3 for Imaging of Histone

Deacetylases 1 and 2 in Brain.

Pharmaceuticals **2022**, *15*, 324.

[https://doi.org/10.3390/](https://doi.org/10.3390/ph15030324)

[ph15030324](https://doi.org/10.3390/ph15030324)

Academic Editor: Carlos

Alberto Manssour Fraga

Received: 1 February 2022

Accepted: 3 March 2022

Published: 8 March 2022

Publisher's Note: MDPI stays neutral with regard to jurisdictional claims in published maps and institutional affiliations.

Abstract: The degree of acetylation of lysine residues on histones influences the accessibility of DNA and, furthermore, the gene expression. Histone deacetylases (HDACs) are overexpressed in various tumour diseases, resulting in the interest in HDAC inhibitors for cancer therapy. The aim of this work is the development of a novel ¹⁸F-labelled HDAC1/2-specific inhibitor with a benzamide-based zinc-binding group to visualize these enzymes in brain tumours by positron emission tomography (PET). **BA3**, exhibiting high inhibitory potency for HDAC1 (IC₅₀ = 4.8 nM) and HDAC2 (IC₅₀ = 39.9 nM), and specificity towards HDAC3 and HDAC6 (specificity ratios >230 and >2080, respectively), was selected for radiofluorination. The two-step one-pot radiosynthesis of [¹⁸F]BA3 was performed in a TRACERlab FX2 N radiosynthesizer by a nucleophilic aliphatic substitution reaction. The automated radiosynthesis of [¹⁸F]BA3 resulted in a radiochemical yield of 1%, a radiochemical purity of >96% and a molar activity between 21 and 51 GBq/μmol (*n* = 5, EOS). For the characterization of **BA3**, in vitro and in vivo experiments were carried out. The results of these pharmacological and pharmacokinetic studies indicate a suitable inhibitory potency of **BA3**, whereas the applicability for non-invasive imaging of HDAC1/2 by PET requires further optimization of the properties of this compound.

Keywords: histone deacetylase inhibitor; HDAC1/2-specific; radiochemistry; fluorine-18 labelling; positron emission tomography (PET); brain-penetration; glioblastoma; glioma



Copyright: © 2022 by the authors. Licensee MDPI, Basel, Switzerland. This article is an open access article distributed under the terms and conditions of the Creative Commons Attribution (CC BY) license (<https://creativecommons.org/licenses/by/4.0/>).

1. Introduction

Epigenetics describe inheritable and reversible regulation mechanisms of genes expression without altering the DNA sequence. It plays a pivotal role in gene expression by enzyme-mediated post-translational modifications (PTMs) of proteins, such as formylation, methylation, ubiquitination and acetylation. Two of the most studied modifications are the processes of deacetylation and acetylation of lysine side chains on histones, which are regulated by the opposing enzymes histone deacetylases (HDACs) and histone acetyltransferases (HATs). The HDAC family consists of 18 isoforms, which are subdivided into four classes. The enzymes of classes I, II and IV are zinc-dependent enzymes, whereas class

III enzymes, also known as sirtuins, are NAD⁺-dependent (Table 1) [1–3]. The enzymatic deacetylation of lysine residues by HDACs leads to a positive charge on histones, and consequently modulates the chromatin structure by increasing the interaction of histones with the negatively charged phosphate groups of the DNA. The condensed chromatin structure restricts access of transcription factors to the DNA, and thus results in transcriptional repression. Conversely, the acetylation of histones by HATs is associated with a more open, and relaxed chromatin conformation and induced transcriptional activation. Over the past years, accumulating evidence showed that dysregulations of the histone deacetylation mechanism impact, among others, cell proliferation, apoptosis, cell differentiation and inflammation processes. These are associated with the progression of pathophysiological states, such as cancer, neurodegenerative disorders or memory impairment [2–5]. Furthermore, the upregulation of HDACs1/2 was discovered in several types of cancers, including gastric, colorectal, and prostate cancer as well as glioblastoma and several haematological malignancies. Both HDACs share a sequence similarity of around 93% and are usually co-expressed in several large co-repressor complexes, such as NuRD and MiDAC [6–9]. HDACs1/2 were also found to play a critical role in tumorigenesis and are inversely correlated with disease-free intervals and overall survival [4,10–15]. Given their regulatory activity in multiple processes involved in cancer progression and resistance to radiotherapy and chemotherapy, the development of HDAC-targeted therapies using single agents or drug combinations is very attractive for tumour entities presenting a poor prognosis, and treatment resistance such as glioblastoma [16–18]. For these reasons, the use of HDAC inhibitors in the management of gliomas is studied in clinical trials using pan-inhibitors: **valproic acid** (NCT00302159), **panobinostat** (NCT00859222) or **vorinostat** (NCT01236560) as adjuvant therapy to radiotherapy and/or chemotherapy. However, the development of such a personalized therapy would benefit from a non-invasive imaging tool to help (1) assessing the drug targeting potential and (2) to gain more fundamental understanding of the HDAC1/2 density and role in healthy and pathogenic brain tissue, which is still not well understood.

Table 1. Classification of HDACs and their distribution in human according to [2].

Class	Enzymes	Localization	Expression
I	HDAC1, 2, 3, 8	Nucleus	Ubiquitous
IIa	HDAC4, 5, 7, 9	Nucleus and cytoplasm	Tissue specific
IIb	HDAC6, 10	Cytoplasm	Tissue specific
III	Sirtuins 1–7	Variable	Variable
IV	HDAC11	Nucleus and cytoplasm	Ubiquitous

Therefore, we aim to develop a radiotracer for the non-invasive imaging of HDACs1/2 in the brain via positron emission tomography (PET). The evaluation of the expression and distribution patterns in vivo will help to understand the significance of these enzymes in neuronal processes and pathologies such as glioblastoma.

In the last two decades, numerous HDAC inhibitors and radiotracers have been developed, but only a few were able to cross the blood–brain barrier (BBB) and exhibit suitable pharmacokinetics for brain imaging. HDAC inhibitors contain generally a zinc-binding group (ZBG), a linker and a cap group, visualized in Figure 1 on the structures of published inhibitors. Over the years hydroxamic acids and benzamides have emerged as the most frequently used ZBGs.

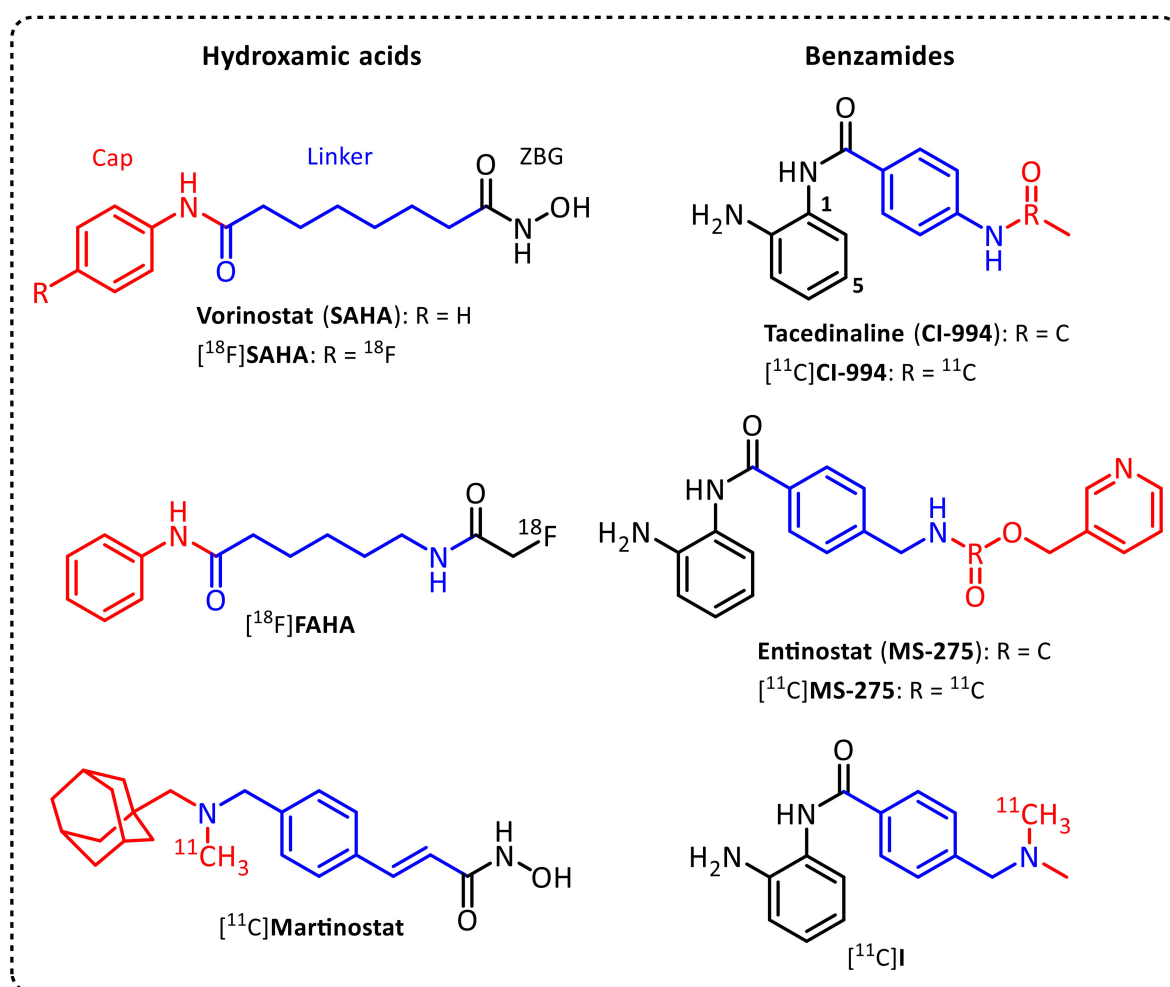


Figure 1. Pharmacophore model and structures of selected hydroxamic acids and benzamides as HDAC inhibitors and their corresponding PET radiotracers.

Hydroxamic-acid-based radiotracers such as [^{18}F]SAHA [19] and [^{18}F]FAHA [20–25], structurally based on the FDA-approved drug vorinostat (SAHA) [26], showed either poor BBB penetration ([^{18}F]SAHA) or acted as a substrate for HDACs and thus was metabolized rapidly in vivo ([^{18}F]FAHA). Characterized as pan-HDAC inhibitors, these compounds notoriously lack selectivity towards specific HDAC isoforms or classes. In 2014, the cinnamoyl hydroxamic acid [^{11}C]martinostat was developed as an HDAC1, 2, 3 and 6-specific radiotracer with good BBB penetration [27–30]. In contrast, benzamide-based inhibitors such as tacedinaline and entinostat (see Figure 1) generally demonstrate selectivity towards class I HDACs and do not show genotoxicity [31–34]. Consequently, radiolabelled benzamide inhibitors have emerged as an alternative to hydroxamic acids for the diagnostic imaging of class I HDACs in brain via PET. Nevertheless, there are only a few benzamide-based radiotracers published. Additionally, both the ^{11}C -radiolabelled HDAC1-3-specific inhibitors tacedinaline [^{11}C]CI-994 [35] and entinostat [^{11}C]MS-275 [36] showed a low brain uptake in vivo. However, while developing a series of benzamide-based brain-penetrable radiotracers, it was discovered that a benzylic amine, e.g., in [^{11}C]I (Figure 1), is responsible for an improved brain uptake [35]. Furthermore, the specificity towards HDAC1, as well as HDAC2, can be improved by a substitution on the 5-position of the 2-aminoanilide structure (see Figure 1) with a (hetero)aromatic moiety. Such bulky, lipophilic moieties are able to engage the so-called “foot pocket”, an internal cavity in these enzymes [37–41].

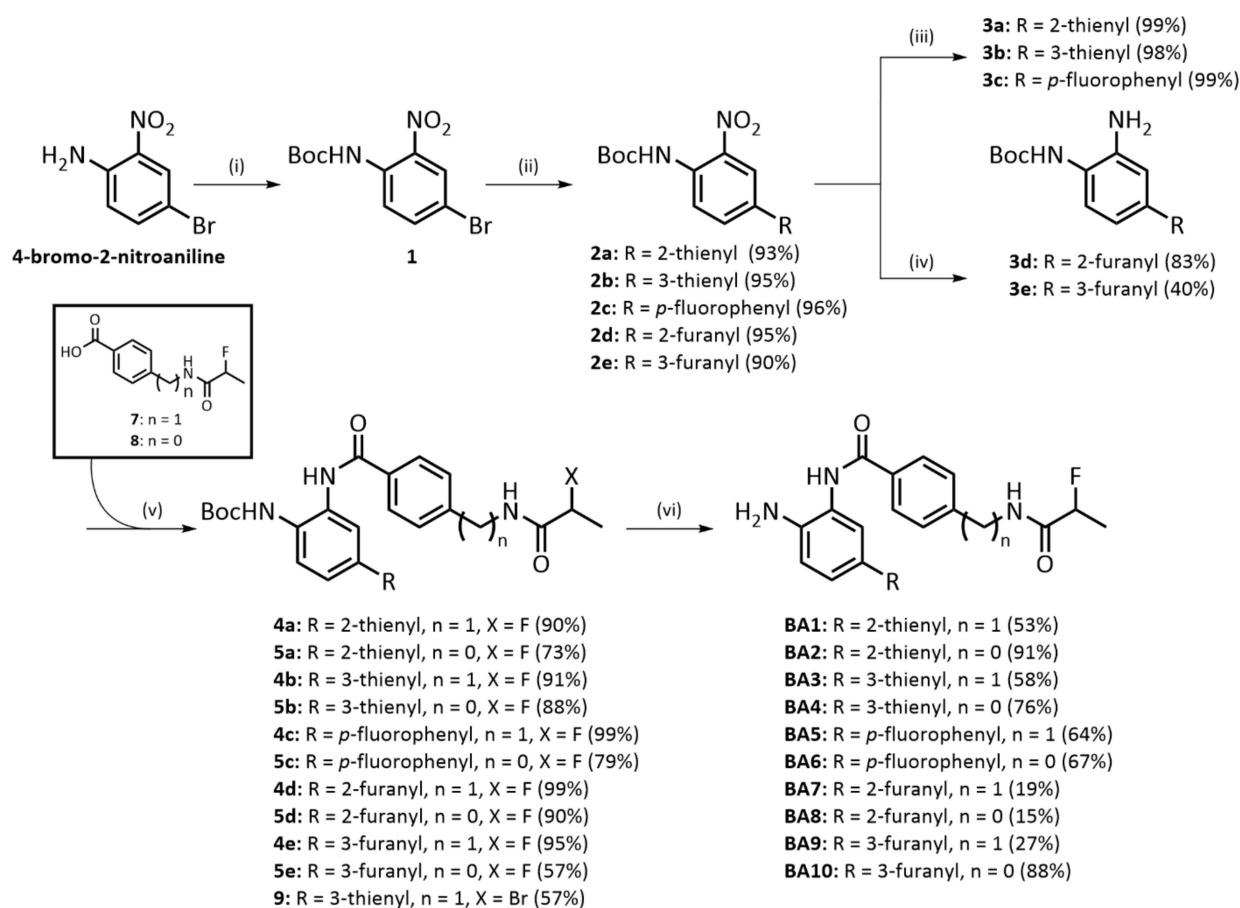
The aim of this work is the development of a novel ^{18}F -labelled HDAC1/2-specific inhibitor with a benzamide-based ZBG for targeting these enzymes in brain tumours. Therefore, a series of fluorinated compounds, based on entinostat and tacedinaline, bearing

bulky, lipophilic moieties on the 5-position of the *ortho*-aminoanilide scaffold, to increase the specificity towards the HDACs1/2, was designed. Subsequently, the designed compounds were synthesized and their inhibitory potencies against HDAC1, 2, 3 and 6 were determined. The most potent compound was radiofluorinated and biologically evaluated regarding its in vitro cell toxicity in different brain tumour cell lines as well as its in vivo metabolism and pharmacokinetics.

2. Results and Discussion

2.1. Organic Chemistry

A small library of new compounds (**BA1–BA10**) was synthesized using a six-step synthesis route (Scheme 1). As fluorine-bearing moiety the 2-fluoropropanamide was used instead of the apparently obvious fluoroacetamide moiety. The [¹⁸F]fluoroacetamido group is known to suffer from limited stability in vivo and to carry the risk of defluorination [22,23,42,43]. Both processes would be disadvantageous for imaging by PET. In contrast, the 2-[¹⁸F]fluoropropanoyl group is used frequently for PET tracer design, due to higher metabolic stability [44–47]. Additionally, it is expected to have a low impact on biological activity due to its small size.



Scheme 1. Synthetic strategy. (i) (1) Boc₂O, TEA, DMAP, THF, r.t., 4 h; (2) TFA, DCM, r.t., 6 h; (ii) boronic acid, Pd(PPh₃)₄, K₂CO₃, 1,4-dioxane/water 7:3 (v/v), 110 °C, 2.5 h; (iii) H₂, 10% Pd/C, MeOH/EA 1:1 (v/v), r.t., 8 h; (iv) Na₂S₂O₄, NaHCO₃, dioxane/water 5:1 (v/v), 110 °C, 1 h; (v) for compounds **4a–e**, **5a–e**: 7/8, PyBOP, DIPEA, DMF, r.t., 12 h; for compound **9**: (1) 4-(Fmoc-aminomethyl)benzoic acid, PyBOP, DIPEA, DMF, r.t., 12 h; (2) 20% piperidine in DMF, r.t., 4 h; (3) 2-bromopropanoyl bromide, TEA, DCM, r.t., 2.5 h; (vi) 30% TFA in DCM, r.t., 2 h.

Starting from 4-bromo-2-nitroaniline, the Boc protection of the aromatic amino group was performed in two steps [48]. First of all, the amino group was treated with di-*tert*-butyl

dicarbonate (Boc₂O) and catalytic amounts of *N,N*-dimethyl-4-aminopyridine (DMAP) to afford the bis-Boc-protected intermediate followed by cleavage of one Boc group using trifluoroacetic acid (TFA) to give *tert*-butyl (4-bromo-2-nitrophenyl)carbamate (**1**) in a total yield of 95%. Under these conditions it was possible to achieve higher yields with this two-step synthesis compared with the reported yields [49–53] using a one-step synthesis. Subsequently, **1** was reacted with 2-/3-thienyl-, 2-/3-furanyl- or *para*-fluoro-phenylboronic acid in a Suzuki cross coupling reaction with tetrakis(triphenylphosphine)palladium(0) (Pd(PPh₃)₄) in 1,4-dioxane/water (7:3, *v/v*) to provide the corresponding compounds **2a–e** in very good yields (90–96%). In the first approach, the reduction in the aromatic nitro group was carried out under hydrogen atmosphere with palladium on carbon and afforded **3a–c** in quantitative yields [49]. Using the same procedure for the 3-furan-containing compound **2e**, the desired aniline product could not be obtained. The NMR analysis showed that both, the aromatic nitro group and the 3-furan, were entirely reduced to form the corresponding aniline derivative substituted with 3-tetrahydrofuran instead of 3-furan. Therefore, a reduction by sodium dithionite was carried out as a milder alternative, which gave the desired products **3d** and **3e** in good to moderate yields (83% and 40%, respectively) [54]. Subsequently, the amide couplings of **3a** and **3b** with 4-(Fmoc-aminomethyl)benzoic acid were performed in a straight forward synthesis under standard conditions using (benzotriazol-1-yloxy)tripyrrolidinophosphonium hexafluorophosphate (PyBOP) as coupling reagent. After cleaving the Fmoc protecting group with a solution of 20% piperidine in *N,N*-dimethylformamide (DMF), the resulting amines were coupled with 2-fluoropropanoic acid under the same reaction conditions and led to the compounds **4a** and **4b** (23% and 40%, respectively, over three steps). To bypass the use of protecting groups and increase the yield of the amide coupling, we synthesized the 4-[(2-fluoropropanamido)methyl]- and 4-(2-fluoropropanamido)benzoic acids **7** and **8** by acylation of the amino group of 4-(aminomethyl)-(PAMBA) and 4-aminobenzoic acid (PABA) with 2-fluoropropanoyl chloride **6** in good yields (63% and 79%, respectively). With the compounds **7** and **8** we were then able to perform the final amide coupling in one instead of three reaction steps to synthesize the corresponding compounds **4a–e** and **5a–e** in better yields (57–95%). Finally, the Boc protecting group was removed with a solution of 30% TFA in dichloromethane (DCM) to give the final products **BA1–BA10** after precipitation in moderate to good yields (15–91%).

2.2. Determination of the In Vitro Inhibitory Potency

All prepared compounds as well as the reference HDAC inhibitors **vorinostat**, **entinostat** and **tacedinaline** were tested regarding their inhibitory activity against the class I enzymes HDAC1–3. Additionally, HDAC6 was used as a control isoform to evaluate the selectivity towards class IIb HDACs. The IC₅₀ values are shown in Table 2.

The HDAC inhibitors containing (hetero)aryl substituted benzamides as ZBG showed, as expected, a high inhibitory activity against HDAC1 with IC₅₀ values ranging from 4.8 nM to 24.2 nM for **BA1–BA10**. In contrast, negligibly low inhibitions of HDAC3 and HDAC6 were observed. The screening also revealed that the compounds with the PAMBA linker (*n* = 1, **BA1/BA3/BA5/BA7**), compared with the PABA linker (*n* = 0, **BA2/BA4/BA6/BA8**), have a higher inhibitory potency towards HDAC1. The only exceptions are **BA9** and **BA10**, which both bear a 3-furan substitution and exhibit no substantial differences in the IC₅₀ values against HDAC1. Compared with the approved hydroxamic acid-based HDAC inhibitor **vorinostat** and the benzamides **tacedinaline** and **entinostat**, the inhibitory potencies of the new compounds are significantly improved towards HDAC1. It is known that the use of a foot pocket-targeting (hetero)aromatic substituent at position 5 of the aminoanilide moiety leads to an increase in the specificity for HDAC1 and HDAC2 over HDAC3 [37–41]. This could be proven by the specificity ratios (HDAC1/HDAC3) determined for the synthesized compounds ranging from >74 (**BA6**) to 479 (**BA1**) compared with nearly no specificity of the reference compounds **vorinostat**, **entinostat** or **tacedinaline**, respectively. Out of the series, **BA1** and **BA3** showed the best inhibitory activities

against HDAC1. **BA3** was selected for radiolabelling as the most active inhibitor of HDAC1 and HDAC2.

Table 2. Determined inhibitory activities of **BA1-BA10** against HDAC1-3 and 6.

Compound	R	n	IC ₅₀ [nM]			
			HDAC1	HDAC2	HDAC3	HDAC6
BA1	2-thienyl	1	4.8 ± 0.4	64.3 ± 4.5	2300 ± 190	>10,000 ^a
BA2	2-thienyl	0	8.3 ± 1.4	33.5 ± 1.5	>1110 ^b	>10,000 ^a
BA3	3-thienyl	1	4.8 ± 0.6	39.9 ± 3.2	>1110 ^b	>10,000 ^a
BA4	3-thienyl	0	11.2 ± 2.4	38.1 ± 4.5	>3330 ^b	>10,000 ^a
BA5	4-fluorophenyl	1	10.2 ± 0.4	32.2 ± 5.5	1300 ± 70	>10,000 ^a
BA6	4-fluorophenyl	0	14.9 ± 0.4	56.6 ± 0.6	>1110 ^b	>10,000 ^a
BA7	2-furanyl	1	20.4 ± 0.3	69.1 ± 1.2	3800 ± 180	>10,000 ^a
BA8	2-furanyl	0	24.2 ± 2.9	82.1 ± 0.1	4200 ± 80	>10,000 ^a
BA9	3-furanyl	1	19.8 ± 0.4	56.3 ± 0.2	2400 ± 250	>10,000 ^a
BA10	3-furanyl	0	17.0 ± 1.2	47.7 ± 2.9	3300 ± 480	>10,000 ^a
vorinostat	-	-	124 ± 15	197 ± 14	129 ± 7	22 ± 3
entinostat ^c	-	-	426 ± 59	354 ± 43	311 ± 10	>10,000 ^a
tacedinaline	-	-	636 ± 114	696 ± 11	263 ± 31	>10,000 ^a

^a < 10% inhibition at 10,000 nM; ^b < 30% inhibition at the given concentration; ^c data taken from reference [55].

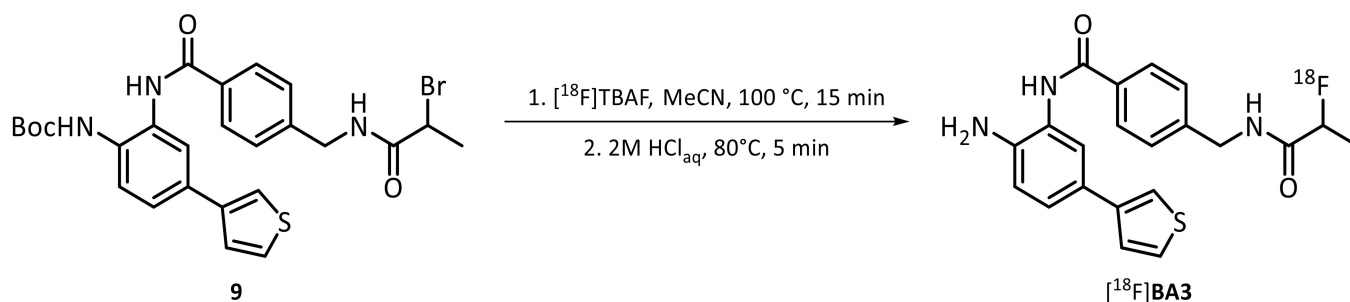
2.3. Precursor- and Radiosynthesis

2.3.1. Manual Radiosynthesis

For a direct radiofluorination of [¹⁸F]**BA3**, the corresponding Boc-protected bromine precursor **9** was synthesized as shown in Scheme 1 in an overall yield of 34%. The radiolabelling process was investigated under thermal heating using 2–3 mg of precursor **9** and different (i) polar aprotic solvents, (ii) bases, (iii) different precursor to base ratios, (iv) temperatures, (v) reaction times and (vi) azeotropically dried ¹⁸F-fluorination agents. First, the conventional K[¹⁸F]F-K_{2.2.2} was used for radiofluorination of the intermediate Boc-[¹⁸F]**BA3** in DMF, dimethyl sulfoxide (DMSO) and acetonitrile (MeCN) as solvents. The reactions were carried out at 150 °C (DMF/DMSO) or 100 °C (MeCN) for up to 20 min. Aliquots of the reaction mixtures were taken every 5 min and analysed by radio-thin layer chromatography (radio-TLC) and/or radio-reversed phase high-performance liquid chromatography (radio-RP-HPLC) to determine the radiochemical yield (RCY) of the labelling process. In DMF or DMSO with K₂CO₃ as base, the radiosynthesis of Boc-[¹⁸F]**BA3** was not possible. According to radio-RP-HPLC, under these reaction conditions a polar radioactive by-product was formed in high amounts (30% in DMF, 45% in DMSO). When using MeCN as a solvent, it was possible to obtain Boc-[¹⁸F]**BA3** in labelling yields between 1% and 2% (with KHCO₃ or K₂CO₃, respectively), but the same radioactive by-product (~10%) was formed as shown by radio-RP-HPLC. The use of K₂C₂O₄ instead of KHCO₃/K₂CO₃ and 18-crown-6 instead of K_{2.2.2} did not result in an increase in the radiochemical yield of Boc-[¹⁸F]**BA3**. Finally, the additional impact of microwave irradiation, which was investigated in DMSO, DMF and MeCN, respectively, did not improve the radiofluorination. For all syntheses, the (radio-)RP-HPLC chromatograms showed a decomposition of precursor **9** and Boc-[¹⁸F]**BA3** already after 5 min, as well as a large amount of unreacted [¹⁸F]fluoride.

In general, these conditions are strongly basic, limiting the synthetic utility for base-sensitive precursors since various side reactions, such as eliminations, can occur [56]. Assuming that the reaction conditions described above are not suitable for radiosynthesis of Boc-[¹⁸F]**BA3**, the use of [¹⁸F]tetra-*n*-butylammonium fluoride ([¹⁸F]TBAF) was investigated as a milder reagent [57]. The impact of (i) different solvents, (ii) temperatures, and (iii) reaction times were studied. The radiofluorination of Boc-[¹⁸F]**BA3** was investigated first in MeCN at 100 °C achieving labelling yields up to 7% after 15 min, which were not increasing with further reaction time. Then, the influence of *tert*-butanol (*tert*-BuOH) as a solvent at 100 °C was investigated and a labelling yield of 5% was achieved after

20 min. Due to the fact that Boc- ^{18}F BA3 was obtained in highest labelling yields with MeCN, the use of this solvent was kept for further evaluation. The second step after the radiofluorination of Boc- ^{18}F BA3 was the cleavage of the Boc protecting group, which was performed by addition of an aqueous solution of 2 M hydrochloric acid (HCl_{aq}) to the crude mixture of Boc- ^{18}F BA3 and heating at 80 and 100 °C. At 80 °C the reaction was already completed after 5 min as detected by radio-TLC. Finally, the novel radioligand ^{18}F BA3 could be prepared in a two-step one-pot reaction by a direct aliphatic nucleophilic substitution, starting with the precursor **9** and subsequent Boc deprotection under the optimized reaction conditions as shown in Scheme 2.



Scheme 2. Optimized reaction conditions for the radiosynthesis of ^{18}F BA3.

2.3.2. Automated Radiosynthesis

An automated radiosynthesis of ^{18}F BA3 was established based on the optimized reaction conditions using the radiosynthesis module TRACERlab FX2 N. The detailed configuration is shown in the Supplemental part (Figure S1). Briefly, ^{18}F fluoride (starting activities of 7–32 GBq) was trapped on a QMA cartridge and eluted into the reactor with TBAHCO₃ dissolved in MeCN/H₂O and dried via azeotropic distillation. The nucleophilic substitution of the bromine precursor **9** (4 mg) was performed using ^{18}F TBAF in MeCN at 100 °C for 15 min. The subsequent Boc deprotection was carried out by adding an aqueous 2 M HCl solution and stirring for 5 min at 80 °C. After neutralization with a 1 M solution of aqueous NaHCO₃, the radiolabelled product ^{18}F BA3 was isolated via semi-preparative RP-HPLC (Figure 2) and purified by solid-phase extraction (SPE) on a C18 cartridge. Subsequent elution with ethanol (EtOH) and formulation in sterile 0.9% saline containing 10% of EtOH reproducibly provided ^{18}F BA3 in a total synthesis time of approximately 85 min with RCYs of $0.9 \pm 0.2\%$ (EOB, $n = 5$; see Figure S2 for UV- and radio-RP-HPLC-chromatograms of formulated ^{18}F BA3). The identity of ^{18}F BA3 was confirmed by analytical radio- and UV-RP-HPLC of the final product, co-injected with the reference compound BA3 (Figure 2). Finally, the radiotracer was obtained with a radiochemical purity of >96% and a molar activity in the range of 21–51 GBq/ μmol (EOS, $n = 5$).

2.4. Lipophilicity and Radiochemical Stability of ^{18}F BA3

The distribution coefficient ($\log D_{7.4}$) was experimentally determined by the shake-flask method in the *n*-octanol/PBS system. The $\log D_{7.4}$ value of 1.75 ± 0.16 ($n = 8$) for ^{18}F BA3 suggests that a moderate passive diffusion through the BBB is most likely [58–60]. The radiotracer ^{18}F BA3 was stable in *n*-octanol, as well as in the saline formulation containing 10% EtOH at room temperature for more than two hours (radiochemical purity > 99%).

2.5. In Vivo PET/MRI Studies of ^{18}F BA3

The pharmacokinetics of ^{18}F BA3 was investigated by dynamic PET scans on healthy CD-1 mice in order to evaluate the passage across the BBB, nonspecific binding and thus the expected background level. The time–activity curve (TAC) of the brain (peak standardized uptake value (SUV) at 0.8 min of ~ 0.16) demonstrates a low brain uptake (see Figure 3 and Figure S4). Further radiotracer accumulation reaches a plateau at 15 min (~ 0.22 SUV)

followed by a slow washout reaching a SUV of ~ 0.16 at 60 min after i.v. administration. Notably, only 21% of the parent compound was found in the brain at 30 min p.i., suggesting that the major part of the measured activity originates from the nonspecific accumulation of radiometabolites.

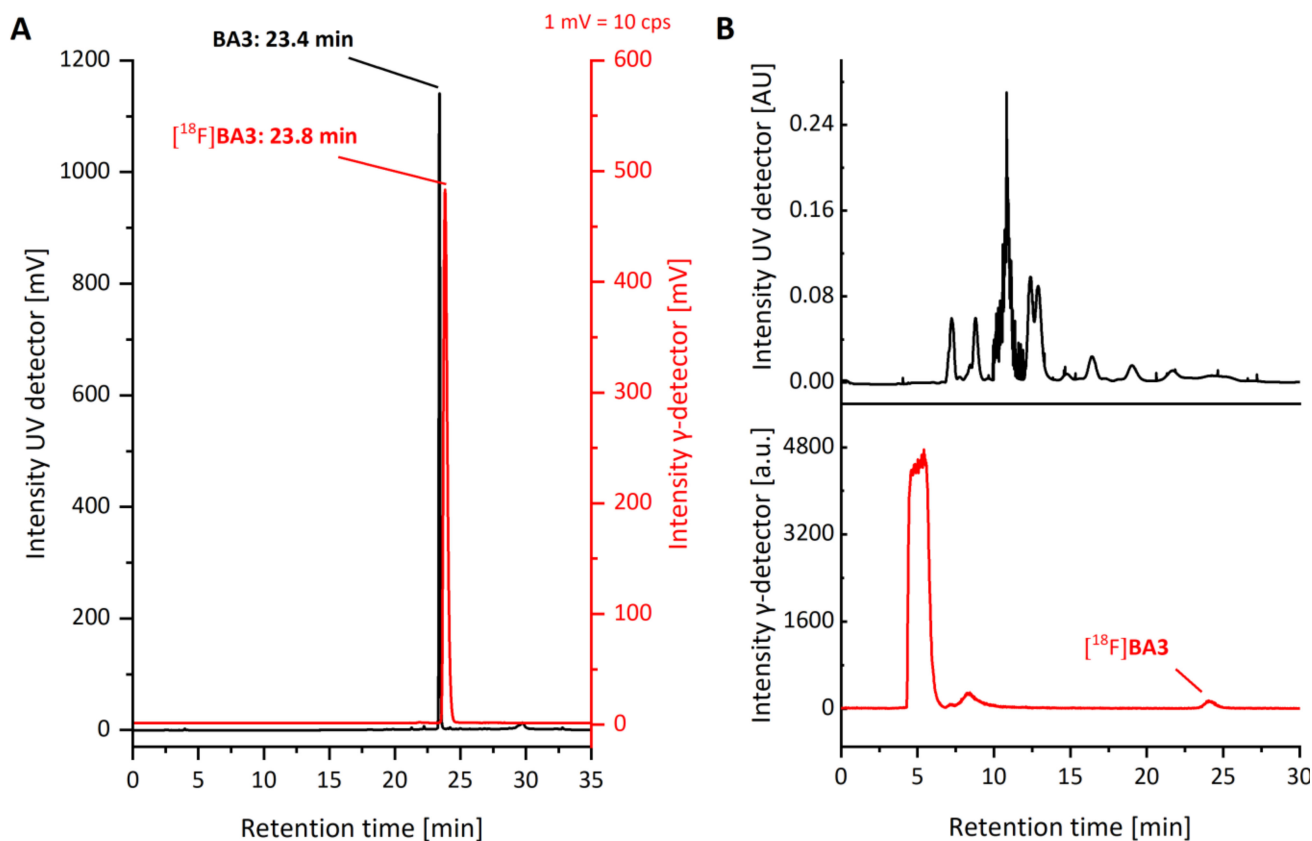


Figure 2. (A) Analytical radio- and UV-RP-HPLC chromatograms of formulated $[^{18}\text{F}]\text{BA3}$ spiked with the corresponding reference compound **BA3** (ReproSil-Pur 120 C18-AQ column (250×4.6 mm, $5 \mu\text{m}$), Gradient MeCN/ $20 \text{ mM NH}_4\text{OAc}_{\text{aq}}$, (see quality control), flow rate: 1 mL/min ; red: radio-RP-HPLC chromatogram, black: UV-RP-HPLC chromatogram); and (B) Radio- and UV-RP-HPLC chromatograms obtained for the isolation of $[^{18}\text{F}]\text{BA3}$ by semipreparative RP-HPLC (ReproSil-Pur 120 C18-AQ (250×10 mm, $10 \mu\text{m}$), $40\% \text{ MeCN}/20 \text{ mM NH}_4\text{OAc}_{\text{aq}}$, flow rate: 4 mL/min ; AU = absorption unit, a.u. = arbitrary unit; red: radio-RP-HPLC chromatogram, black: UV-RP-HPLC chromatogram).

Although these first results do not support favourable imaging features of $[^{18}\text{F}]\text{BA3}$, the evaluation of its potential affinity to efflux drug transporter present at the BBB could help to predict the features of other derivatives of this class of compound. Thus, pre-administration of **cyclosporine A**, an inhibitor of the P-glycoprotein (P-gp) efflux transporter, increased the initial uptake of $[^{18}\text{F}]\text{BA3}$ by about factor two (0.18 vs. 0.42 SUV) indicating that $[^{18}\text{F}]\text{BA3}$ is a substrate of P-gp.

Evaluation of the whole-body distribution derived from PET imaging revealed a low accumulation of tracer and/or metabolites in spleen, kidney, muscle, liver, and small intestines (initial uptake: $\text{SUV}_{5 \text{ min}} < 4$), as well as a relatively constant activity in blood circulation ($\text{SUV}_{5 \text{ min}}$ to $\text{SUV}_{60 \text{ min}}$: 1.47 vs. 1.10). An elevated accumulation occurred in the gallbladder and the bladder, indicating both urinary and hepatobiliary excretion (Figures S5 and S6 and Table S1).

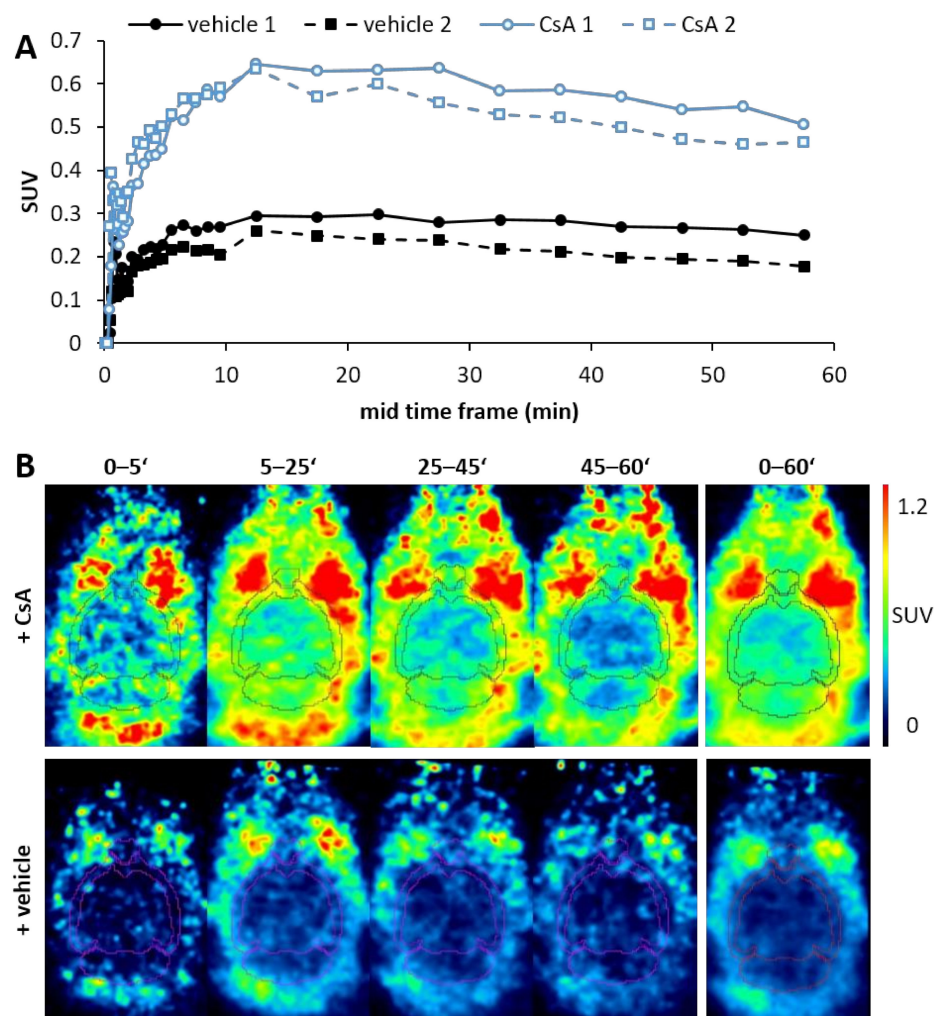


Figure 3. (A) Time–activity curves (TACs) of CD-1 mice brain region after pre-administration of vehicle ($n = 2$; black line) or cyclosporine A (CsA; P-gp inhibitor, 50 mg/kg, $n = 2$; blue line) 30 min pre-injection of [^{18}F]BA3. (B) Horizontal representative PET image of the brain after pre-administration of vehicle or CsA.

In conclusion, although [^{18}F]BA3 presents a high *in vitro* inhibitory potency towards HDAC1 ($\text{IC}_{50} = 4.8 \pm 0.6 \text{ nM}$) and HDAC2 ($\text{IC}_{50} = 39.9 \pm 3.2 \text{ nM}$), and an excellent specificity of HDAC1 over HDAC3 and HDAC6 (specificity ratios >230 and >2080 , respectively), its low passage across the BBB and the presence of radiometabolites in brain show the need for further ligand optimization.

2.6. *In Vivo* Metabolism of [^{18}F]BA3

The *in vivo* metabolism of [^{18}F]BA3 was investigated in the plasma, brain homogenate and urine obtained from mice at 30 min after injection into the tail vein. The radiometabolites and parent compound were analysed by (i) analytical radio-RP-HPLC and (ii) radio-micellar chromatography (radio-MLC) [61]. Prior to the analysis with radio-RP-HPLC, the plasma and brain samples were treated with MeCN/ H_2O (9:1, *v/v*) as extraction solvent. The recovery of activity in plasma and brain samples was 97% and 95%, respectively. Radio-RP-HPLC analysis revealed that the intact radiotracer accounted for about 5% and 21% (mean, $n = 2$) of the total activity in plasma and brain, respectively. Similar results were obtained with MLC (about 6% and 24% (mean, $n = 2$) in plasma and brain, respectively), where the samples are directly injected without previous protein precipitation (for corresponding MLC chromatograms see Figure S3). In urine intact radiotracer was not detected by neither radio-RP-HPLC nor radio-MLC. In the corresponding radio-chromatograms

(Figure 4) five radiometabolites ($[^{18}\text{F}]\text{M1}$ - $[^{18}\text{F}]\text{M5}$) were detected in brain at 30 min p.i. In contrast, in plasma one single major radiometabolite, $[^{18}\text{F}]\text{M4}$, amounting to 74%, was found. However, a conclusion, whether the radiometabolites in the brain originate from the plasma and pass the blood–brain barrier or are formed within the brain itself, was not possible, as only a single time point was investigated.

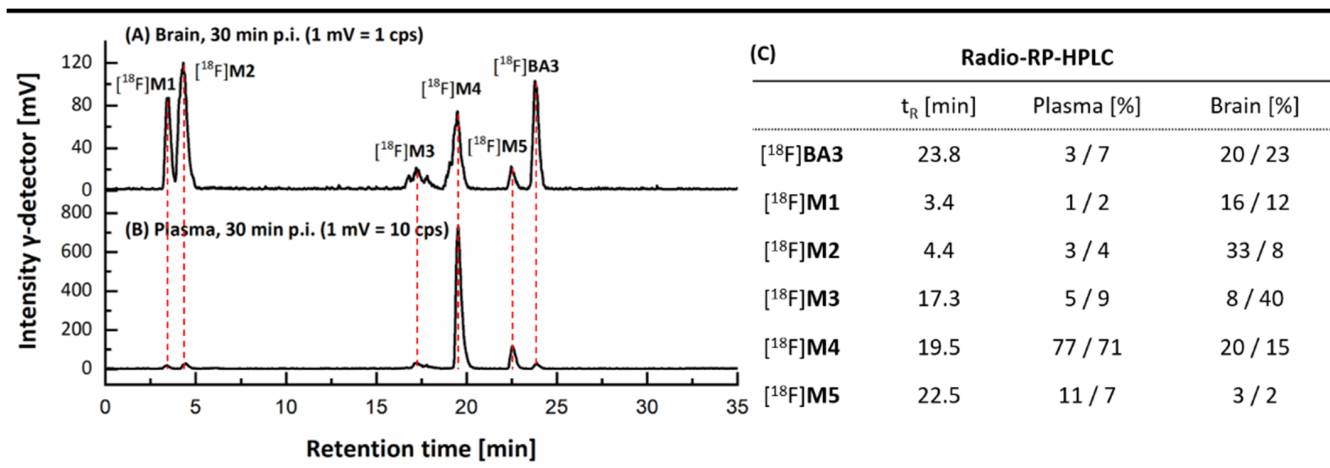


Figure 4. (A,B) Representative radio-RP-HPLC chromatograms of in vivo metabolism studies from brain and plasma samples obtained 30 min p.i. of $[^{18}\text{F}]\text{BA3}$ in a CD-1 mouse ($[^{18}\text{F}]\text{M1}$ - $[^{18}\text{F}]\text{M5}$: radiometabolites detected in brain; gamma-detection via radio-RP-HPLC: ReproSil-Pur 120 C18-AQ column (250 × 4.6 mm, 5 μm), Gradient MeCN/20 mM $\text{NH}_4\text{OAc}_{\text{aq}}$. (see quality control), flow: 1 mL/min) and (C) the amount of radiometabolites in percent ($n = 2$).

2.7. Expression of HDAC1 in F98 and U251-MG Cells

The expression of HDAC1 was evaluated by immunofluorescence microscopy of the glioblastoma cell lines F98 and U251-MG to check whether they are suitable for the assessment of the toxicity of HDAC inhibitors. As shown in Figure 5, both cell lines possess a HDAC1 nuclear localization, proved by the merged signals of the HDAC1 (green) enzyme and the nuclei (blue). Interestingly, the HDAC1 signal is exactly co-localized with the nuclei in the F98 cells but additionally presents a slight cytoplasmic localization in U251-MG cells, as also previously found by Seto et al. [62].

2.8. The New HDAC Inhibitor BA3 Has Potential to Reduce the Proliferation of Cancer Cells

Inhibition of HDAC activity has been shown to hinder the proliferation of cancer cells. To assess the cytotoxic potential of **BA3**, the effect of this compound on the proliferation of the rat glioma F98 cells and the human glioblastoma U251-MG cells in comparison with the well-established HDAC inhibitors **tacedinaline**, **vorinostat**, and **entinostat** was investigated by an MTS assay (Table 3). Although solubility problems detected only after completion of the study (slight precipitation of **BA3** at 50 μM in cell culture medium supplemented with 0.5% DMSO) preclude the direct comparison of the cytotoxic potency between the established HDAC inhibitors and **BA3**, the similar strongly diminished viability of F98 and U251-MG cells induced by **BA3** at a concentration of even lower than 50 μM indicate nevertheless a high cytotoxic potential of **BA3**. Thus, although differently designed studies would be needed to determine proper cytotoxic IC_{50} values and even though not relevant for imaging studies performed with radiotracers at low to sub-nanomolar concentrations, the presented data suggest, that the pharmacological potency of **BA3** is at least comparable if not even higher than that of established and clinically tested HDAC inhibitors.

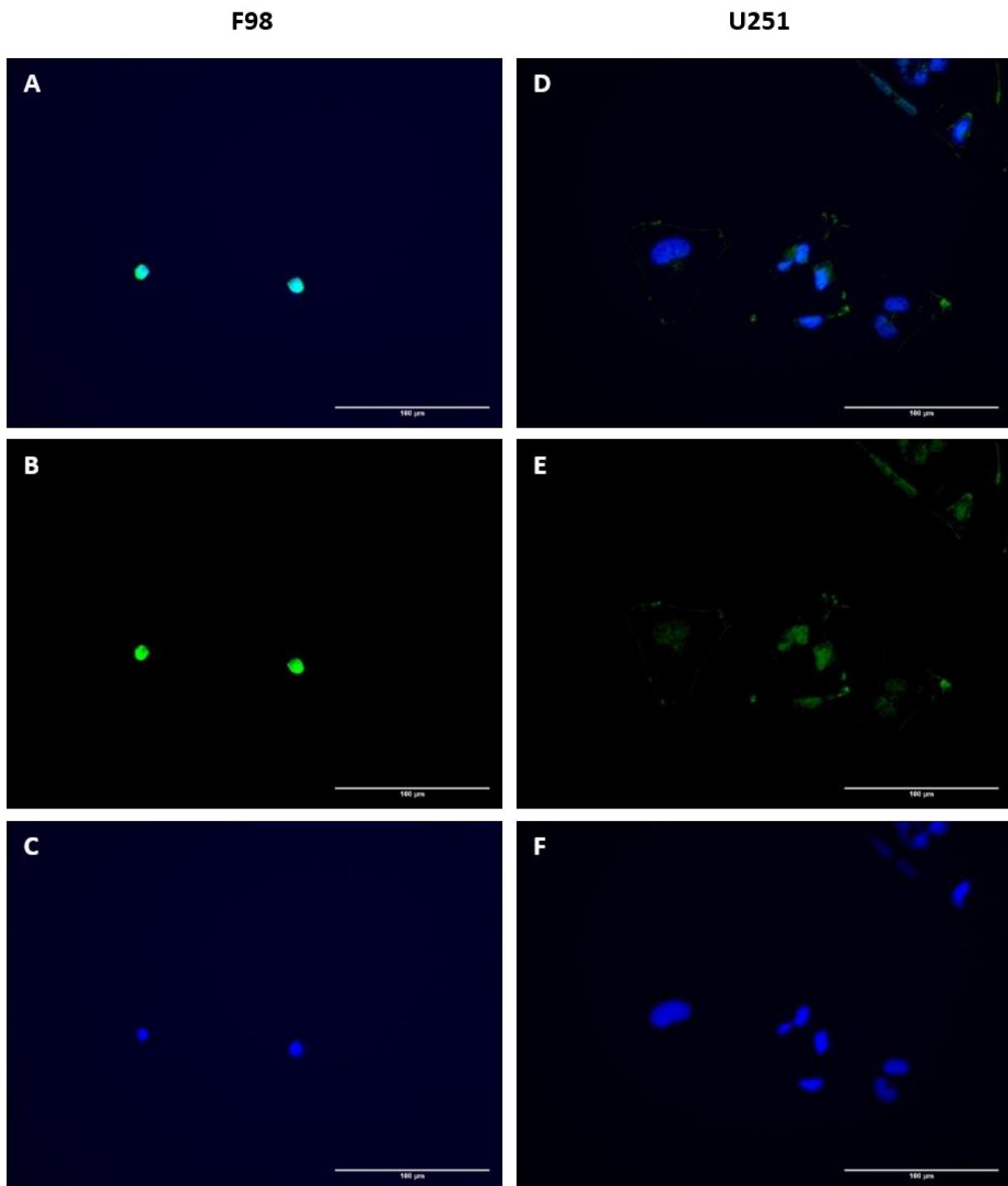


Figure 5. Immunofluorescent staining of HDAC1 enzyme. Representative images of the HDAC1 staining in (A–C) F98 cells and (D–F) U251 cells. (A,D) pictures displays the merged channels, (B,E) the green channel only and (C,F) the blue channel only. (Scale bar: 100 µm, magnification $\times 40$, green channel: HDAC1 staining, blue channel: nuclei staining).

Table 3. Effect of **BA3** and reference HDAC inhibitors on cancer cell viability. Viability of rat F98 glioma cells and human U251-MG glioblastoma cells was measured by MTS assay (CellTiter 96[®] AQUEOUS One Solution Cell Proliferation Assay; Promega GmbH, Walldorf, Germany) after incubation with <50 μM **BA3** or 50 μM reference HDAC inhibitors for 72 h. The results are expressed in relation to vehicle (0.5% DMSO, considered as 100% viability) as the mean percentage \pm standard deviation ($n = 3$; each experiment performed in quintuplicate).

HDAC Inhibitor (conc.)	Cell Viability [%] (Vehicle = 100%)	
	U251-MG	F98
BA3 (< 50 μM ^a)	63.6 \pm 20.7	36.3 \pm 7.6
vorinostat (50 μM)	36.9 \pm 7.6	24.4 \pm 7.9
entinostat (50 μM)	55.0 \pm 11.2	27.5 \pm 4.4
tacedinaline (50 μM)	28.5 \pm 3.0	27.1 \pm 3.0

^a precipitation of **BA3** at 50 μM visible under microscope, exact concentration unknown.

3. Materials and Methods

3.1. General

Chemicals were purchased from commercial suppliers in analytical grade and used without further purification. Solvents were dried before use, if required. Air- and moisture-sensitive reactions were carried out under inert gas atmosphere using argon. The reaction monitoring was carried out by (radio-)TLC on pre-coated silica gel plates (Alugram[®] Xtra SIL G/UV254; Polygram[®] SIL G/UV254) purchased from Macherey-Nagel (Düren, Germany). The compounds were visualized with UV light at $\lambda = 254$ nm and 365 nm and/or by staining with aqueous KMnO_4 solution or ninhydrin solution.

The UV purity of the final compounds **BA1–BA10** was determined by LC-MS on an UltiMate 3000 UHPLC System (Thermo Scientific, Germering, Germany) including a DAD detector (DAD-3000RS) coupled to an MSQ Plus Single Quadrupole Mass Spectrometer (Thermo Scientific, Austin, TX, USA). LC-MS analyses were performed on a ReproSil-Pur 120 C18-AQ-column (150 mm \times 3 mm, 3 μm ; Dr. Maisch GmbH, Ammerbuch, Germany) equipped with an appropriate precolumn in gradient mode (0–1.5 min: 5% MeCN/20 mM NH_4OAc , 1.5–8 min: 5% \rightarrow 80% MeCN/20 mM NH_4OAc , 8–12 min: 80% MeCN/20 mM NH_4OAc , 12–12.5 min: 80% \rightarrow 5% MeCN/20 mM NH_4OAc , 12.5–15 min: 5% MeCN/20 mM NH_4OAc) and a flow of 0.7 mL/min. UV detection was performed at a wavelength of 254 nm and used for determination of UV purity by calculation of the relative peak area. MSQ Plus single quadrupole mass spectrometer was operated in positive electrospray ionization mode: probe temperature 500 $^\circ\text{C}$, needle voltage 5 V and cone voltage 75 V.

NMR spectra (^1H , ^{13}C , ^{19}F) were recorded on Mercury 300/Mercury 400 (Varian, Palo Alto, CA, USA) or Fourier 300/Avance DRX 400 Bruker (Billerica, MA, USA) instruments. The hydrogenated residue of deuterated solvents and/or tetramethylsilane (TMS) were used as internal standards for ^1H -NMR (CDCl_3 , $\delta = 7.26$; $\text{DMSO-}d_6$, $\delta = 2.50$) and ^{13}C -NMR (CDCl_3 , $\delta = 77.16$; $\text{DMSO-}d_6$, $\delta = 39.52$). The chemical shifts (δ) are reported in ppm (s, singlet; brs, broad singlet; d, doublet; t, triplet; q, quartet; m, multiplet) and the corresponding coupling constants (J) are reported in Hz. High resolution mass spectra (ESI +/−) were recorded on an Esquire 3000Plus instrument (Bruker Daltonics, Billerica, MA, USA; equipped with ion trap). The ^1H -, ^{13}C - and ^{19}F -NMR spectra and LC-MS chromatograms for compounds **BA1–BA10** are displayed in Figures S7–S46

3.2. General Procedures

3.2.1. Suzuki Coupling **A1**

An aqueous solution of K_2CO_3 (2.6 eq.) was added to a solution of **1** (1 eq.) and the respective boronic acid (1.2 eq.) in 1,4-dioxane under argon atmosphere. After addition of tetrakis(triphenylphosphine)palladium(0) (0.05 eq.), the mixture was stirred under reflux until the complete consumption of **2**. The 1,4-dioxane was evaporated; the crude product

was dissolved in ethyl acetate (EA) and washed with water and brine. After drying over Na_2SO_4 the solvent was evaporated and the product purified by flash chromatography.

3.2.2. Nitro Reduction with Hydrogen **A2a**

The nitro compound was dissolved in EA and diluted with MeOH (1:1, *v/v*). After flushing with argon, Pd/C (0.05 eq., 10% *wt/wt*) was added and the mixture was stirred under hydrogen atmosphere at room temperature for 12 h. The solvent was removed, the crude product was adsorbed on silica and purified by flash chromatography.

3.2.3. Nitro Reduction with Sodium Dithionite **A2b**

To a solution of nitro compound (1 eq.) in 1,4-dioxane/water (5:1, *v/v*), sodium dithionite (4 eq.) and sodium bicarbonate (10 eq.) were added. The heterogeneous mixture was stirred vigorously under reflux until the complete consumption of the nitro compound. The salts were filtered off and 1,4-dioxane evaporated. The organic compounds were transferred in a separation funnel with EA and H_2O , extracted twice with EA, washed with brine, and dried over Na_2SO_4 . After evaporation, the crude product was purified by flash chromatography.

3.2.4. Amide Coupling **A3**

To a solution of the carboxylic acid and *N,N*-diisopropylethylamine (DIPEA) in DMF, PyBOP was added in small portions and subsequently stirred for 30 min at room temperature. In the meantime, a solution of the respective amine in DMF was prepared and then added to the stirring solution. After stirring overnight most of the DMF was evaporated, the residue was dissolved in EA, washed with water and brine, and dried over Na_2SO_4 . After adsorbing the crude product on silica, it was purified by flash chromatography.

3.2.5. Boc Cleavage **A4**

For the cleavage of the Boc group the corresponding compound (1 eq.) was dissolved in a 30% TFA (20 eq.) solution in DCM and stirred for 2–4 h. The solution was diluted with EA, washed extensively with a 5% aqueous solution of NaHCO_3 and dried over Na_2SO_4 . The EA was removed until the product started to precipitate. Ice-cold heptane was added, and the product was filtered off and dried under reduced pressure.

3.3. Compounds

3.3.1. Synthesis of *tert*-butyl (4-bromo-2-nitrophenyl)carbamate (**1**)

To a solution of 4-bromo-2-nitroaniline (10 g, 46 mmol, 1 eq.) in 150 mL THF, TEA (15.9 mL, 115 mmol, 2.5 eq.) and DMAP (1.1 g, 9.2 mmol, 0.2 eq.) were added successively. While stirring at room temperature, the first portion Boc_2O (10 g, 46 mmol, 1 eq.) was added until it was completely dissolved. Then the second portion Boc_2O (11.6 g, 53 mmol, 1.15 eq.) was added in smaller portions and the solution was stirred at room temperature for 4 h. The reaction volume was reduced to a third and an aqueous solution of citric acid (29 g, 151 mmol) was added. After extraction of the compound with EA, the organic layer was dried over Na_2SO_4 and the solvent was evaporated to give a light-yellow solid. The crude product was dissolved in a solution of TFA (5.3 mL, 69 mmol, 1.5 eq.) in 140 mL DCM and stirred for 6 h. The reaction was monitored by TLC and after completion an aqueous solution of NaHCO_3 (6.7 g, 80 mmol) was added, the product was extracted twice with DCM, washed with brine, and dried over Na_2SO_4 . It was purified by flash chromatography (silica, gradient PE/EA 20:1 → 18:1 → 16:1) to give **1** as yellow solid (13.93 g, 95%).

$^1\text{H-NMR}$ (400 MHz, CDCl_3) δ 9.60 (s, 1H), 8.51 (d, $J = 9.2$ Hz, 1H), 8.33 (d, $J = 2.4$ Hz, 1H), 7.68 (dd, $J = 9.2, 2.4$ Hz, 1H), 1.54 (s, 9H); $^{13}\text{C-NMR}$ (101 MHz, CDCl_3) δ 152.09, 138.67, 136.32, 135.28, 128.40, 122.35, 113.88, 82.45, 28.32 (in accordance with literature [53]).

3.3.2. Synthesis of *tert*-butyl [2-nitro-4-(thiophen-2-yl)phenyl]carbamate (**2a**)

Compound **1** (2 g, 6.3 mmol) and 2-thienylboronic acid in 25 mL 1,4-dioxane, K_2CO_3 in 11 mL H_2O and catalyst were reacted according to the general procedure **A1** to give after purification by flash chromatography (silica, gradient PE/EA: 25:1 → 20:1 → 15:1) compound **2a** (1.88 g, 93%) as yellow solid.

1H -NMR (400 MHz, $CDCl_3$) δ 9.65 (s, 1H), 8.59 (d, J = 9.0 Hz, 1H), 8.40 (d, J = 2.3 Hz, 1H), 7.82 (dd, J = 8.9, 2.3 Hz, 1H), 7.37–7.30 (m, 2H), 7.10 (dd, J = 5.1, 3.6 Hz, 1H), 1.56 (s, 9H); ^{13}C -NMR (101 MHz, $CDCl_3$) δ 152.27, 141.49, 136.20, 134.96, 133.07, 128.88, 128.46, 125.81, 124.08, 122.52, 121.35, 82.17, 28.36 (in accordance with literature [53]).

3.3.3. Synthesis of *tert*-butyl [2-nitro-4-(thiophen-3-yl)phenyl]carbamate (**2b**)

Compound **1** (3 g, 9.46 mmol) and 3-thienylboronic acid in 38 mL 1,4-dioxane, K_2CO_3 in 17 mL H_2O and catalyst were reacted according to the general procedure **A1** to give after purification by flash chromatography (silica, gradient PE/EA: 24:1 → 19:1 → 14:1 → 9:1) compound **2b** (2.87 g, 95%) as yellow solid.

1H -NMR (400 MHz, $CDCl_3$) δ 9.65 (s, 1H), 8.60 (d, J = 8.9 Hz, 1H), 8.40 (d, J = 2.2 Hz, 1H), 7.83 (dd, J = 8.9, 2.3 Hz, 1H), 7.50 (dd, J = 2.9, 1.4 Hz, 1H), 7.45–7.35 (m, 2H), 1.56 (s, 9H); ^{13}C -NMR (101 MHz, $CDCl_3$) δ 152.33, 139.55, 136.25, 134.78, 133.62, 130.16, 127.16, 125.90, 123.08, 121.27, 121.21, 82.07, 28.36.

3.3.4. Synthesis of *tert*-butyl (4'-fluoro-3-nitro-[1,1'-biphenyl]-4-yl)carbamate (**2c**)

Compound **1** (1 g, 3.15 mmol) and 4-fluorophenylboronic acid in 15 mL 1,4-dioxane, K_2CO_3 in 5 mL H_2O and catalyst were reacted according to the general procedure **A1** to give after purification by flash chromatography (silica, gradient PE/EA: 25:1 → 11.5:1 → 4:1) compound **2c** (1.0 g, 96%) as white solid.

1H -NMR (400 MHz, $CDCl_3$) δ 9.66 (s, 1H), 8.63 (d, J = 8.9 Hz, 1H), 8.37 (d, J = 2.3 Hz, 1H), 7.79 (dd, J = 8.9, 2.3 Hz, 1H), 7.59–7.50 (m, 2H), 7.21–7.10 (m, 2H), 1.56 (s, 9H); ^{19}F -NMR (377 MHz, $CDCl_3$) δ -114.12 (ddd, J = 13.8, 8.6, 5.2 Hz); ^{13}C -NMR (76 MHz, $CDCl_3$) δ 162.98 (d, J = 247.9 Hz), 152.35, 136.34, 135.08, 134.51 (d, J = 3.2 Hz), 134.28, 134.12, 128.55 (d, J = 8.2 Hz), 123.73, 121.41, 116.21 (d, J = 21.7 Hz), 82.16, 28.36 (in accordance with literature [55]).

3.3.5. Synthesis of *tert*-butyl [4-(furan-2-yl)-2-nitrophenyl]carbamate (**2d**)

Compound **1** (2 g, 6.3 mmol) and 2-furanylboronic acid in 25 mL 1,4-dioxane, K_2CO_3 in 11 mL H_2O and catalyst were reacted according to the general procedure **A1** to give after purification by flash chromatography (silica, gradient PE/EA: 30:1 → 20:1 → 10:1) compound **2d** (1.83 g, 95%) as orange solid.

1H -NMR (400 MHz, $CDCl_3$) δ 9.68 (s, 1H), 8.62 (d, J = 8.9 Hz, 1H), 8.48 (d, J = 2.1 Hz, 1H), 7.88 (dd, J = 8.9, 2.2 Hz, 1H), 7.52 (dd, J = 1.8, 0.7 Hz, 1H), 6.72 (dd, J = 3.4, 0.8 Hz, 1H), 6.52 (dd, J = 3.4, 1.8 Hz, 1H), 1.58 (s, 9H); ^{13}C -NMR (101 MHz, $CDCl_3$) δ 152.28, 151.53, 142.87, 136.25, 134.77, 130.92, 125.37, 121.19, 120.66, 112.08, 106.12, 82.12, 28.36.

3.3.6. Synthesis of *tert*-butyl [4-(furan-3-yl)-2-nitrophenyl]carbamate (**2e**)

Compound **1** (2 g, 6.3 mmol) and 3-furanylboronic acid in 25 mL 1,4-dioxane, K_2CO_3 in 11 mL H_2O and catalyst were reacted according to the general procedure **A1** to give after purification by flash chromatography (silica, gradient PE/EA: 30:1 → 20:1 → 10:1) compound **2d** (1.73 g, 90%) as orange solid.

1H -NMR (400 MHz, $CDCl_3$) δ 9.63 (s, 1H), 8.57 (d, J = 8.9 Hz, 1H), 8.27 (d, J = 2.2 Hz, 1H), 7.77 (t, J = 1.2 Hz, 1H), 7.70 (dd, J = 8.9, 2.2 Hz, 1H), 7.53–7.48 (m, 1H), 6.70 (dd, J = 2.0, 0.9 Hz, 1H), 1.55 (s, 9H); ^{13}C -NMR (101 MHz, $CDCl_3$) δ 152.35, 144.35, 139.07, 136.30, 134.70, 133.17, 126.96, 124.39, 122.54, 121.34, 108.61, 82.09, 28.37.

3.3.7. Synthesis of *tert*-butyl [2-amino-4-(thiophen-2-yl)phenyl]carbamate (**3a**)

The reduction in compound **2a** (1.5 g, 4.7 mmol) was performed according to the general procedure **A2a** in 60 mL EA/MeOH (1:1, *v/v*) to give after purification by flash chromatography (silica, gradient PE/EA: 6:1 → 4:1 → 3:1 → 1:1) compound **3a** (1.37 g) as white-beige solid in quantitative yield.

¹H-NMR (400 MHz, DMSO-*d*₆) δ 8.34 (s, 1H), 7.44 (dd, *J* = 5.1, 1.2 Hz, 1H), 7.32–7.24 (m, 2H), 7.08 (dd, *J* = 5.1, 3.6 Hz, 1H), 6.98 (d, *J* = 2.2 Hz, 1H), 6.84 (dd, *J* = 8.2, 2.2 Hz, 1H), 5.01 (s, 2H), 1.47 (s, 9H); ¹³C-NMR (101 MHz, DMSO-*d*₆) δ 153.48, 144.01, 141.20, 130.18, 128.21, 124.55, 123.51, 122.42, 113.65, 112.40, 78.83, 28.15 (in accordance with literature [49]).

3.3.8. Synthesis of *tert*-butyl [2-amino-4-(thiophen-3-yl)phenyl]carbamate (**3b**)

The reduction in compound **2b** (1.0 g, 3.12 mmol) was performed according to the general procedure **A2a** in 50 mL EA/MeOH (1:1, *v/v*) to give after purification by flash chromatography (silica, gradient PE/EA: 6:1 → 4:1 → 3:1 → 1:1) compound **3b** (890 mg, 98%) as white-beige solid.

¹H-NMR (400 MHz, DMSO-*d*₆) δ 8.32 (s, 1H), 7.66–7.54 (m, 2H), 7.38 (dd, *J* = 5.0, 1.4 Hz, 1H), 7.25 (d, *J* = 8.2 Hz, 1H), 7.01 (d, *J* = 2.1 Hz, 1H), 6.88 (dd, *J* = 8.2, 2.1 Hz, 1H), 4.90 (s, 2H), 1.47 (s, 9H); ¹³C-NMR (101 MHz, DMSO-*d*₆) δ 153.54, 141.82, 141.12, 131.75, 126.70, 125.99, 124.47, 123.09, 119.54, 114.46, 113.18, 78.73, 28.16.

3.3.9. Synthesis of *tert*-butyl (3-amino-4'-fluoro-[1,1'-biphenyl]-4-yl)carbamate (**3c**)

The reduction in compound **2c** (1.0 g, 3.0 mmol) was performed according to the general procedure **A2a** in 50 mL EA/MeOH (1:1, *v/v*) to give after purification by flash chromatography (silica, gradient PE/EA: 4:1 → 1.5:1 → 1:1) compound **3c** (895 mg) as white-beige solid in quantitative yield.

¹H-NMR (300 MHz, CDCl₃) δ 7.52–7.43 (m, 2H), 7.34 (d, *J* = 7.8 Hz, 1H), 7.13–7.03 (m, 2H), 6.99–6.90 (m, 2H), 6.24 (s, 1H), 3.85 (s, 2H), 1.53 (s, 9H); ¹⁹F-NMR (282 MHz, CDCl₃) δ –116.04 (¹H decoupled); ¹³C-NMR (75 MHz, CDCl₃) δ 162.94 (d, *J* = 246.1 Hz), 153.96, 140.23, 138.41, 137.15, 128.59 (d, *J* = 8.02 Hz), 125.11, 124.31, 118.56, 116.25, 115.63 (d, *J* = 21.38 Hz), 80.86, 28.48 (in accordance with literature [55]).

3.3.10. Synthesis of *tert*-butyl [2-amino-4-(furan-2-yl)phenyl]carbamate (**3d**)

The reduction in compound **2d** (1.78 g, 5.85 mmol) was performed according to the general procedure **A2b** in 42 mL 1,4-dioxane/H₂O (5:1, *v/v*) to give after purification by flash chromatography (silica, gradient PE/EA: 4:1 → 2:1 → 1:1) compound **3d** (1.34 g, 83%) as white-beige solid.

¹H-NMR (400 MHz, CDCl₃) δ 7.42 (dd, *J* = 1.8, 0.8 Hz, 1H), 7.32 (d, *J* = 8.3 Hz, 1H), 7.14–7.07 (m, 2H), 6.55 (dd, *J* = 3.4, 0.8 Hz, 1H), 6.44 (dd, *J* = 3.4, 1.8 Hz, 1H), 6.26 (s, 1H), 3.77 (s, 2H), 1.52 (s, 9H); ¹³C-NMR (101 MHz, CDCl₃) δ 153.90, 153.86, 141.88, 139.86, 128.80, 124.70, 124.46, 115.71, 113.03, 111.71, 104.73, 80.80, 28.47 (in accordance with literature [63]).

3.3.11. Synthesis of *tert*-butyl [2-amino-4-(furan-3-yl)phenyl]carbamate (**3e**)

The reduction in compound **2e** (1.68 g, 5.52 mmol) was performed according to the general procedure **A2b** in 42 mL 1,4-dioxane/H₂O (5:1, *v/v*) to give after purification by flash chromatography (silica, gradient PE/EA: 4:1 → 2:1 → 1:1) compound **3e** (611 mg, 40%) as white-beige solid.

¹H-NMR (400 MHz, CDCl₃) δ 7.65 (dd, *J* = 1.6, 0.9 Hz, 1H), 7.45–7.43 (m, 1H), 7.27 (d, *J* = 8.0 Hz, 1H), 6.95–6.86 (m, 2H), 6.63 (dd, *J* = 1.9, 0.9 Hz, 1H), 6.23 (s, 1H), 3.42 (brs, 2H), 1.52 (s, 9H); ¹³C-NMR (101 MHz, CDCl₃) δ 153.98, 143.63, 140.27, 138.45, 130.55, 126.25, 125.21, 123.91, 117.52, 115.06, 109.04, 80.77, 28.47.

3.3.12. Synthesis of *tert*-butyl (2-{4-[(2-fluoropropanamido)methyl]benzamido}-4-[thiophen-2-yl]phenyl)carbamate (**4a**)

Compound **7** (20 mg, 0.089 mmol, 1 eq.), compound **3a** (29 mg, 0.098 mmol, 1.1 eq.), DIPEA (34 μ L, 0.2 mmol, 2.3 eq.) and PyBOP (56 mg, 0.107 mmol, 1.2 eq.) in 1 mL DMF were reacted according to the general procedure **A3** to give after purification by flash chromatography (silica, gradient PE/EA: 3:1 \rightarrow 2:1) compound **4a** (40 mg, 90%) as brownish foam.

$^1\text{H-NMR}$ (400 MHz, CDCl_3) δ 9.35 (s, 1H), 7.96–7.87 (m, 3H), 7.35–7.25 (m, 4H), 7.24–7.19 (m, 2H), 7.16 (s, 1H), 7.05–6.98 (m, 1H), 6.82 (d, $J = 5.5$ Hz, 1H), 5.06 (dq, $J = 49.3$, 6.8 Hz, 1H), 4.51 (d, $J = 6.0$ Hz, 2H), 1.61 (dd, $J = 24.8$, 6.8 Hz, 3H), 1.48 (s, 9H); $^{19}\text{F-NMR}$ (377 MHz, $\text{DMSO-}d_6$) δ –181.13 (dq, $J = 51.5$, 25.6, 19.3 Hz); $^{13}\text{C-NMR}$ (101 MHz, CDCl_3) δ 171.00 (d, $J = 19.2$ Hz), 165.68, 154.69, 143.34, 141.89, 133.40, 132.10, 130.88, 129.64, 128.10, 128.07, 127.76, 124.96, 123.55, 123.45, 122.98, 88.98 (d, $J = 182.9$ Hz), 81.44, 42.62, 28.38, 18.65 (d, $J = 21.5$ Hz); HRFT-MS (ESI+): $m/z = 995.3654$ (calc. 995.3642 for $[2\text{M}+\text{H}]^+$).

3.3.13. Synthesis of *tert*-butyl (2-{4-[(2-fluoropropanamido)methyl]benzamido}-4-[thiophen-3-yl]phenyl)carbamate (**4b**)

Compound **7** (12 mg, 0.053 mmol, 1 eq.), compound **3b** (17 mg, 0.058 mmol, 1.1 eq.), DIPEA (21 μ L, 0.122 mmol, 2.3 eq.) and PyBOP (34 mg, 0.064 mmol, 1.2 eq.) in 1 mL DMF were reacted according to the general procedure **A3** to give after a rough purification by flash chromatography (silica, gradient PE/EA: 3:1 \rightarrow 2:1) compound **4b** (24 mg, 91%) as brownish foam.

$^1\text{H-NMR}$ (400 MHz, CDCl_3) δ 9.34 (s, 1H), 7.95–7.86 (m, 3H), 7.36–7.22 (m, 7H), 7.08 (s, 1H), 6.79 (d, $J = 5.4$ Hz, 1H), 5.05 (dq, $J = 49.3$, 6.8 Hz, 1H), 4.50 (d, $J = 6.0$ Hz, 2H), 1.60 (dd, $J = 24.8$, 6.8 Hz, 3H), 1.47 (s, 9H); $^{19}\text{F-NMR}$ (377 MHz, $\text{DMSO-}d_6$) δ –181.16 (tdd, $J = 53.1$, 44.7, 25.2 Hz); $^{13}\text{C-NMR}$ (101 MHz, CDCl_3) δ 170.98 (d, $J = 19.3$ Hz), 165.60, 154.77, 141.89, 141.27, 133.62, 133.49, 130.97, 129.22, 128.05, 127.79, 126.36, 126.27, 124.95, 123.99, 123.62, 120.53, 88.99 (d, $J = 182.8$ Hz), 81.43, 42.63, 28.40, 18.65 (d, $J = 21.5$ Hz); HRFT-MS (ESI+): $m/z = 1017.3456$ (calc. 1017.3461 for $[2\text{M}+\text{Na}]^+$).

3.3.14. Synthesis of *tert*-butyl (4'-fluoro-3-{4-[(2-fluoropropanamido)methyl]benzamido}-[1,1'-biphenyl]-4-yl)carbamate (**4c**)

Compound **7** (100 mg, 0.444 mmol, 1 eq.), compound **3c** (174 mg, 0.577 mmol, 1.3 eq.), DIPEA (184 μ L, 1.021 mmol, 2.3 eq.) and PyBOP (277 mg, 0.533 mmol, 1.2 eq.) in 12 mL DMF were reacted according to the general procedure **A3** to give after a rough purification by flash chromatography (silica, gradient PE/EA: 9:1 \rightarrow 4:1 \rightarrow 1:1) the crude compound **4c** (300 mg, 132% mass balance). It was used without further purification for following reactions.

$^1\text{H-NMR}$ (300 MHz, $\text{DMSO-}d_6$) δ 9.89 (s, 1H), 8.79 (d, $J = 9.7$ Hz, 2H), 7.98–7.89 (m, 2H), 7.84 (d, $J = 2.2$ Hz, 1H), 7.76–7.60 (m, 3H), 7.50 (dd, $J = 8.5$, 2.2 Hz, 1H), 7.42 (d, $J = 8.3$ Hz, 2H), 7.34–7.25 (m, 2H), 5.09 (dq, $J = 48.9$, 6.7 Hz, 1H), 4.40 (d, $J = 6.1$ Hz, 2H), 1.47 (dd, $J = 24.5$, 6.7 Hz, 3H), 1.47 (s, 9H); $^{19}\text{F-NMR}$ (282 MHz, $\text{DMSO-}d_6$) δ –115.65 (ddd, $J = 14.1$, 9.0, 5.3 Hz), –181.12 (dd, $J = 48.9$, 24.3 Hz); $^{13}\text{C-NMR}$ (75 MHz, $\text{DMSO-}d_6$) δ 170.02 (d, $J = 20.2$ Hz), 165.29, 161.78 (d, $J = 244.3$ Hz), 153.41, 143.34, 135.81 (d, $J = 3.0$ Hz), 134.82, 132.79, 131.09, 129.95, 128.34 (d, $J = 8.3$ Hz), 127.69, 127.11, 124.07, 124.03, 123.72, 115.75 (d, $J = 21.3$ Hz), 87.96 (d, $J = 179.2$ Hz), 79.79, 41.49, 28.03, 18.46 (d, $J = 21.9$ Hz); HRFT-MS (ESI+): $m/z = 1019.4312$ (calc. 1019.4325 for $[2\text{M}+\text{H}]^+$).

3.3.15. Synthesis of *tert*-butyl (2-{4-[(2-fluoropropanamido)methyl]benzamido}-4-[furan-2-yl]phenyl)carbamate (**4d**)

Compound **7** (130 mg, 0.577 mmol, 1 eq.), compound **3d** (206 mg, 0.75 mmol, 1.3 eq.), DIPEA (238 μ L, 1.327 mmol, 2.3 eq.) and PyBOP (360 mg, 0.692 mmol, 1.2 eq.) in 15 mL DMF were reacted according to the general procedure **A3** to give after a rough purification by

flash chromatography (silica, gradient PE/EA: 10:1 → 8:1 → 4:1 → 1:1) the crude compound **4d** (290 mg, 104%). It was used without further purification for following reactions.

$^1\text{H-NMR}$ (400 MHz, $\text{DMSO-}d_6$) δ 9.87 (s, 1H), 8.84–8.78 (m, 1H), 8.75 (s, 1H), 7.94 (d, $J = 8.3$ Hz, 2H), 7.88 (d, $J = 2.0$ Hz, 1H), 7.73 (dd, $J = 1.8, 0.8$ Hz, 1H), 7.62 (d, $J = 8.6$ Hz, 1H), 7.54 (dd, $J = 8.5, 2.1$ Hz, 1H), 7.42 (d, $J = 8.3$ Hz, 2H), 6.88 (dd, $J = 3.4, 0.8$ Hz, 1H), 6.59 (dd, $J = 3.4, 1.8$ Hz, 1H), 5.09 (dq, $J = 48.9, 6.7$ Hz, 1H), 4.40 (d, $J = 6.2$ Hz, 2H), 1.47 (dd, $J = 24.5, 6.7$ Hz, 3H), 1.46 (s, 9H); $^{19}\text{F-NMR}$ (377 MHz, $\text{DMSO-}d_6$) δ –176.35 (dq, $J = 49.0, 24.6$ Hz); $^{13}\text{C-NMR}$ (101 MHz, $\text{DMSO-}d_6$) δ 170.03 (d, $J = 20.3$ Hz), 165.32, 153.34, 152.47, 143.34, 142.74, 132.76, 131.05, 129.89, 127.73, 127.11, 126.27, 123.98, 120.99, 120.86, 112.10, 105.46, 87.97 (d, $J = 179.2$ Hz), 79.80, 41.50, 28.03, 18.47 (d, $J = 21.9$ Hz); HRFT-MS (ESI+): $m/z = 963.4101$ (calc. 963.4099 for $[\text{2M+H}]^+$).

3.3.16. Synthesis of *tert*-butyl (2-[4-[(2-fluoropropanamido)methyl]benzamido]-4-[furan-3-yl]phenyl)carbamate (**4e**)

Compound **7** (130 mg, 0.577 mmol, 1 eq.), compound **3e** (206 mg, 0.75 mmol, 1.3 eq.), DIPEA (238 μL , 1.327 mmol, 2.3 eq.) and PyBOP (360 mg, 0.692 mmol, 1.2 eq.) in 15 mL DMF were reacted according to the general procedure **A3** to give after a rough purification by flash chromatography (silica, gradient PE/EA: 10:1 → 8:1 → 4:1 → 1:1) the crude compound **4e** (265 mg, 95%). It was used without further purification for following reactions.

$^1\text{H-NMR}$ (400 MHz, $\text{DMSO-}d_6$) δ 9.86 (s, 1H), 8.84–8.74 (m, 1H), 8.65 (s, 1H), 8.14 (dd, $J = 1.6, 0.9$ Hz, 1H), 8.02–7.86 (m, 2H), 7.77–7.69 (m, 2H), 7.60–7.50 (m, 1H), 7.49–7.33 (m, 3H), 6.91 (dd, $J = 1.9, 0.9$ Hz, 1H), 5.09 (ddd, $J = 48.8, 6.7, 5.0$ Hz, 1H), 4.43–4.34 (m, 2H), 1.52–1.40 (m, 12H); $^{19}\text{F-NMR}$ (377 MHz, $\text{DMSO-}d_6$) δ –181.13 (d, $J = 17.6$ Hz); $^{13}\text{C-NMR}$ (101 MHz, $\text{DMSO-}d_6$) δ 170.03 (d, $J = 20.2$ Hz), 165.24, 153.39, 144.31, 143.32, 139.10, 132.74, 130.77, 129.92, 129.38, 127.69, 127.10, 125.18, 123.95, 123.23, 122.99, 108.64, 87.96 (d, $J = 179.4$ Hz), 79.69, 41.50, 28.03, 18.46 (d, $J = 21.7$ Hz); HRFT-MS (ESI+): $m/z = 504.1935$ (calc. 504.1905 for $[\text{M+Na}]^+$).

3.3.17. Synthesis of *tert*-butyl {2-[4-(2-fluoropropanamido)benzamido]-4-(thiophen-2-yl)phenyl}carbamate (**5a**)

Compound **8** (300 mg, 1.42 mmol, 1 eq.), compound **3a** (578 mg, 1.988 mmol, 1.4 eq.), DIPEA (612 μL , 3.408 mmol, 2.4 eq.) and PyBOP (887 mg, 1.704 mmol, 1.2 eq.) in 15 mL DMF were reacted according to the general procedure **A3** to give after purification by flash chromatography (silica, gradient PE/EA: 5:1 → 4:1 → 3:1) the compound **5a** (500 mg, 73%) as brownish foam.

$^1\text{H-NMR}$ (400 MHz, $\text{DMSO-}d_6$) δ 10.38 (d, $J = 1.7$ Hz, 1H), 9.87 (s, 1H), 8.74 (s, 1H), 8.02–7.94 (m, 2H), 7.91–7.85 (m, 2H), 7.84 (d, $J = 2.2$ Hz, 1H), 7.61 (d, $J = 8.5$ Hz, 1H), 7.54–7.49 (m, 2H), 7.46 (dd, $J = 3.6, 1.2$ Hz, 1H), 7.13 (dd, $J = 5.1, 3.6$ Hz, 1H), 5.23 (dq, $J = 48.5, 6.7$ Hz, 1H), 1.56 (dd, $J = 24.5, 6.7$ Hz, 3H), 1.46 (s, 9H); $^{19}\text{F-NMR}$ (377 MHz, $\text{DMSO-}d_6$) δ –179.83 (^1H decoupled); $^{13}\text{C-NMR}$ (101 MHz, $\text{DMSO-}d_6$) δ 168.92 (d, $J = 20.7$ Hz), 164.91, 153.33, 142.68, 141.42, 131.17, 130.07, 129.64, 129.19, 128.56, 128.49, 125.42, 124.15, 123.42, 122.82, 122.59, 119.30, 87.78 (d, $J = 179.1$ Hz), 79.81, 28.02, 18.25 (d, $J = 22.1$ Hz); HRFT-MS (ESI+): $m/z = 967.3345$ (calc. 967.3329 for $[\text{2M+H}]^+$).

3.3.18. Synthesis of *tert*-butyl {2-[4-(2-fluoropropanamido)benzamido]-4-(thiophen-3-yl)phenyl}carbamate (**5b**)

Compound **8** (164 mg, 0.774 mmol, 1.5 eq.), compound **3b** (150 mg, 0.516 mmol, 1 eq.), DIPEA (360 μL , 2.064 mmol, 4 eq.) and PyBOP (540 mg, 1.032 mmol, 2 eq.) in 10 mL DMF were reacted according to the general procedure **A3** to give after purification by flash chromatography (silica, gradient PE/EA: 5:1 → 4:1 → 3:1) the compound **5b** (220 mg, 88%) as brownish foam.

$^1\text{H-NMR}$ (400 MHz, $\text{DMSO-}d_6$) δ 10.38 (d, $J = 1.7$ Hz, 1H), 9.85 (s, 1H), 8.69 (s, 1H), 8.01–7.94 (m, 2H), 7.89–7.84 (m, 3H), 7.81 (dd, $J = 2.9, 1.4$ Hz, 1H), 7.64 (dd, $J = 5.0, 2.9$ Hz, 1H), 7.60 (d, $J = 8.5$ Hz, 1H), 7.56 (dd, $J = 8.5, 2.0$ Hz, 1H), 7.52 (dd, $J = 5.0, 1.4$ Hz, 1H), 5.23 (dq, $J = 48.5, 6.7$ Hz, 1H), 1.55 (dd, $J = 24.6, 6.7$ Hz, 3H), 1.46 (s, 9H); $^{19}\text{F-NMR}$ (377 MHz, $\text{DMSO-}d_6$)

δ –179.84 (^1H decoupled); ^{13}C -NMR (101 MHz, $\text{DMSO-}d_6$) δ 168.91 (d, $J = 20.7$ Hz), 164.83, 153.38, 141.37, 140.66, 131.10, 130.88, 129.94, 129.24, 128.50, 127.14, 126.01, 123.93, 123.70, 123.37, 120.56, 119.30, 87.77 (d, $J = 179.1$ Hz), 79.73, 28.03, 18.25 (d, $J = 22.2$ Hz); HRFT-MS (ESI+): $m/z = 989.3136$ (calc. 989.3148 for $[\text{2M}+\text{Na}]^+$).

3.3.19. Synthesis of *tert*-butyl {4'-fluoro-3-[4-(2-fluoropropanamido)benzamido]-4-yl}carbamate (**5c**)

Compound **8** (100 mg, 0.47 mmol, 1 eq.), compound **3c** (187 mg, 0.616 mmol, 1.3 eq.), DIPEA (196 μL , 1.09 mmol, 2.3 eq.) and PyBOP (296 mg, 0.569 mmol, 1.2 eq.) in 12 mL DMF were reacted according to the general procedure **A3** to give after purification by flash chromatography (silica, gradient PE/EA: 8:1 \rightarrow 7:1 \rightarrow 6:1 \rightarrow 4:1 \rightarrow 2:1 \rightarrow 1:2) the compound **5c** (185 mg, 79%) as brownish foam.

^1H -NMR (400 MHz, $\text{DMSO-}d_6$) δ 10.38 (s, 1H), 9.86 (s, 1H), 8.78 (s, 1H), 8.01–7.94 (m, 2H), 7.88–7.77 (m, 3H), 7.73–7.60 (m, 3H), 7.49 (dd, $J = 8.5, 2.2$ Hz, 1H), 7.33–7.24 (m, 2H), 5.23 (dq, $J = 48.5, 6.7$ Hz, 1H), 1.55 (dd, $J = 24.6, 6.7$ Hz, 3H), 1.47 (s, 9H); ^{19}F -NMR (377 MHz, $\text{DMSO-}d_6$) δ –115.63 (tt, $J = 9.9, 5.4$ Hz), –179.85 (dq, $J = 49.1, 24.4$ Hz); ^{13}C -NMR (101 MHz, $\text{DMSO-}d_6$) δ 168.92 (d, $J = 20.5$ Hz), 164.85, 161.78 (d, $J = 244.2$ Hz), 153.43, 141.40, 135.83, 134.83, 131.10, 130.26, 130.03, 129.26, 128.50, 128.34 (d, $J = 8.1$ Hz), 124.08, 123.68, 119.32, 115.75 (d, $J = 21.3$ Hz), 87.77 (d, $J = 179.1$ Hz), 79.81, 28.03, 18.25 (d, $J = 22.1$ Hz); HRFT-MS (ESI+): $m/z = 991.3996$ (calc. 991.4012 for $[\text{2M}+\text{H}]^+$).

3.3.20. Synthesis of *tert*-butyl {2-[4-(2-fluoropropanamido)benzamido]-4-(furan-2-yl)phenyl}carbamate (**5d**)

Compound **8** (130 mg, 0.616 mmol, 1 eq.), compound **3d** (220 mg, 0.801 mmol, 1.3 eq.), DIPEA (255 μL , 1.417 mmol, 2.3 eq.) and PyBOP (385 mg, 0.739 mmol, 1.2 eq.) in 15 mL DMF were reacted according to the general procedure **A3** to give after purification by flash chromatography (silica, gradient PE/EA: 12:1 \rightarrow 10:1 \rightarrow 8:1 \rightarrow 6:1 \rightarrow 4:1) the compound **5d** (260 mg, 90%) as brownish foam.

^1H -NMR (400 MHz, $\text{DMSO-}d_6$) δ 10.38 (s, 1H), 9.84 (s, 1H), 8.75 (s, 1H), 8.01–7.93 (m, 2H), 7.90–7.82 (m, 3H), 7.75–7.70 (m, 1H), 7.62 (d, $J = 8.5$ Hz, 1H), 7.54 (dd, $J = 8.5, 2.1$ Hz, 1H), 6.88 (dd, $J = 3.4, 0.8$ Hz, 1H), 6.58 (dd, $J = 3.4, 1.8$ Hz, 1H), 5.23 (dq, $J = 48.5, 6.7$ Hz, 1H), 1.56 (dd, $J = 24.5, 6.7$ Hz, 3H), 1.46 (s, 9H); ^{19}F -NMR (377 MHz, $\text{DMSO-}d_6$) δ –179.85 (dq, $J = 48.9, 24.6$ Hz); ^{13}C -NMR (101 MHz, $\text{DMSO-}d_6$) δ 168.92 (d, $J = 20.6$ Hz), 164.88, 153.36, 152.48, 142.73, 141.40, 131.06, 129.97, 129.24, 128.53, 126.29, 124.00, 121.03, 120.80, 119.32, 112.10, 105.45, 87.78 (d, $J = 179.2$ Hz), 79.81, 28.03, 18.26 (d, $J = 22.1$ Hz); HRFT-MS (ESI+): $m/z = 935.3795$ (calc. 935.3786 for $[\text{2M}+\text{H}]^+$).

3.3.21. Synthesis of *tert*-butyl {2-[4-(2-fluoropropanamido)benzamido]-4-(furan-3-yl)phenyl}carbamate (**5e**)

Compound **8** (177 mg, 0.84 mmol, 1 eq.), compound **3e** (300 mg, 1.09 mmol, 1.3 eq.), DIPEA (347 μL , 1.93 mmol, 2.3 eq.) and PyBOP (525 mg, 1 mmol, 1.2 eq.) in 20 mL DMF were reacted according to the general procedure **A3** to give after purification by flash chromatography (silica, gradient PE/EA: 8:2 \rightarrow 7:3 \rightarrow 6:4) the compound **5e** (224 mg, 57%) as brownish foam.

^1H -NMR (300 MHz, $\text{DMSO-}d_6$) δ 10.37 (s, 1H), 9.84 (s, 1H), 8.65 (s, 1H), 8.16–8.14 (m, 1H), 8.02–7.94 (m, 2H), 7.88–7.84 (m, 2H), 7.75–7.72 (m, 2H), 7.57 (d, $J = 8.4$ Hz, 1H), 7.46 (dd, $J = 8.4, 2.1$ Hz, 1H), 6.92 (dd, $J = 1.9, 0.9$ Hz, 1H), 5.23 (dq, $J = 48.5, 6.7$ Hz, 1H), 1.56 (dd, $J = 24.5, 6.7$ Hz, 3H), 1.46 (s, 9H); ^{19}F -NMR (282 MHz, $\text{DMSO-}d_6$) δ –179.85 (dq, $J = 48.9, 24.5$ Hz); ^{13}C -NMR (75 MHz, $\text{DMSO-}d_6$) δ 169.38 (d, $J = 20.7$ Hz), 165.27, 153.85, 144.77, 141.84, 139.57, 131.25, 130.44, 129.68, 128.96, 128.34, 125.65, 124.40, 123.75, 123.41, 119.76, 109.10, 88.24 (d, $J = 179.2$ Hz), 80.16, 28.50, 18.71 (d, $J = 22.1$ Hz); HRFT-MS (ESI+): $m/z = 368.1418$ (calc. 368.1405 for $[\text{M}+\text{H}]^+$ Boc deprotection).

3.3.22. Synthesis of 2-fluoropropanoyl chloride (**6**)

Sodium 2-fluoropropanoate (3 g, 26.3 mmol, 1 eq.) was poured in a two-necked flask, cooled down to 0 °C in an ice bath and stirred vigorously. Phosphorus pentachloride PCl_5 (6 g, 28.9 mmol, 1.1 eq.) was then added in small portions. After the complete addition of PCl_5 the mixture was stirred further at room temperature for 3 h. After distillation (10 cm column, $T_{\text{bath}} = 95\text{--}105$ °C, $T_{\text{B}} = 75\text{--}80$ °C; $T_{\text{B,Lit}} = 80.5\text{--}81$ °C [64]) compound **6** (1.7 g, 58%) was isolated as a clear liquid.

Refractive index $n_{\text{D}}^{20} = 1.384$ ($n_{\text{D}}^{20}\text{Lit} = 1.384$ [64]); $^1\text{H-NMR}$ (400 MHz, CDCl_3) δ 5.14 (dq, $J = 48.6, 6.9$ Hz, 1H), 1.70 (dd, $J = 22.8, 6.9$ Hz, 3H); $^{13}\text{C-NMR}$ (101 MHz, CDCl_3) δ 172.57 (d, $J = 27.5$ Hz), 90.33 (d, $J = 194.0$ Hz), 17.70 (d, $J = 22.2$ Hz) (according to literature [65]).

3.3.23. Synthesis of 4-[(2-fluoropropanamido)methyl]benzoic acid (**7**)

To an ice-cold suspension of **6** (1 g, 9 mmol, 1.2 eq.) and 4-(aminomethyl)benzoic acid (1.14 g, 7.5 mmol, 1 eq.) in 13 mL chloroform, pyridine (730 μL , 9 mmol, 1.2 eq.) was added dropwise. After stirring at room temperature overnight, most of the chloroform was evaporated and the residue dissolved in an aqueous solution of Na_2CO_3 (2.12 g, 20 mmol in 20 mL H_2O). After washing twice with MTBE, the aqueous solution was acidified with 10 mL of a 6 M HCl solution, and the product started to precipitate. After stirring for a while, the solid was filtered off and dried under reduced pressure to give compound **7** (1.06 g, 63%) as white solid.

$^1\text{H-NMR}$ (400 MHz, $\text{DMSO-}d_6$) δ 12.86 (s, 1H), 8.82–8.74 (m, 1H), 7.92–7.88 (m, 2H), 7.38–7.34 (m, 2H), 5.08 (dq, $J = 48.8, 6.7$ Hz, 1H), 4.37 (d, $J = 6.1$ Hz, 2H), 1.46 (dd, $J = 24.5, 6.7$ Hz, 3H); $^{19}\text{F-NMR}$ (377 MHz, $\text{DMSO-}d_6$) δ –181.15 (^1H decoupled); $^{13}\text{C-NMR}$ (101 MHz, $\text{DMSO-}d_6$) δ 170.04 (d, $J = 20.2$ Hz), 167.16, 144.32, 129.39, 129.34, 127.14, 87.96 (d, $J = 179.2$ Hz), 41.53, 18.46 (d, $J = 21.9$ Hz).

3.3.24. Synthesis of 4-(2-fluoropropanamido)benzoic acid (**8**)

To an ice-cold suspension of **6** (1 g, 9 mmol, 1.2 eq.) and 4-aminobenzoic acid (1.03 g, 7.5 mmol, 1.2 eq.) in 13 mL chloroform, pyridine (730 μL , 9 mmol, 1.2 eq.) was added dropwise. After stirring at room temperature overnight, most of the chloroform was evaporated and the residue dissolved in an aqueous solution of Na_2CO_3 (2.12 g, 20 mmol in 20 mL H_2O). After washing twice with MTBE, the aqueous solution was acidified with 10 mL of a 6 M HCl solution and the product started to precipitate. After stirring for a while, the solid was filtered off and dried under reduced pressure to give compound **8** (1.25 g, 79%) as white solid.

$^1\text{H-NMR}$ (400 MHz, $\text{DMSO-}d_6$) δ 12.74 (s, 1H), 10.36 (s, 1H), 7.97–7.85 (m, 2H), 7.84–7.76 (m, 2H), 5.21 (dq, $J = 48.5, 6.7$ Hz, 1H), 1.53 (dd, $J = 24.5, 6.7$ Hz, 3H); $^{19}\text{F-NMR}$ (377 MHz, $\text{DMSO-}d_6$) δ –179.89 (^1H decoupled); $^{13}\text{C-NMR}$ (101 MHz, $\text{DMSO-}d_6$) δ 168.95 (d, $J = 20.7$ Hz), 166.86, 142.20, 130.27, 125.88, 119.30, 87.73 (d, $J = 179.0$ Hz), 18.27 (d, $J = 22.2$ Hz).

3.3.25. Synthesis of *tert*-butyl (2-{4-[(2-bromopropanamido)methyl]benzamido}-4-[thiophen-3-yl]phenyl)carbamate (**9**)

To a solution of 4-(Fmoc-aminomethyl)benzoic acid (350 mg, 0.94 mmol, 1 eq.) and DIPEA (337 μL , 1.87 mmol, 2 eq.) in 7 mL DMF, PyBOP (536 mg, 1.03 mmol, 1.1 eq.) was added in small portions. After stirring the mixture for 30 min, a solution of **3b** (355 mg, 1.22 mmol, 1.3 eq.) in 3 mL DMF was added and the solution was stirred at r.t. overnight. The amount of the DMF was reduced by evaporation, the residue was dissolved in EA, washed with water and brine and the organic phase was dried over Na_2SO_4 . A filtration over a silica pad (silica, gradient PE/EA: 10:0 \rightarrow 9:1 \rightarrow 4:1) gave the crude Fmoc-protected compound (830 mg, 137%, mass balance) which was used without further analytics. The Fmoc-protected compound (830 mg, 0.94 mmol) was dissolved in 5 mL of a 20% piperidine solution in DMF and stirred at r.t. for 4 h. The amount of the DMF was reduced by evaporation, the residue was dissolved in EA, washed with water

and brine and the organic phase dried over Na_2SO_4 . After flash chromatography (silica, gradient DCM/MeOH: 100:0 \rightarrow 99:1 \rightarrow 95:5 \rightarrow 90:10) the amine (240 mg, 60%) was used directly for the next reaction. To a solution of the amine (240 mg, 0.57 mmol, 1 eq.) and TEA (87 μL , 0.62 mmol, 1.1 eq.) in 4 mL DCM, 2-bromopropanoyl bromide (135 mg, 0.62 mmol, 1.1 eq.) was added. After stirring the mixture for 2.5 h, the solvent was evaporated and the crude product was purified by flash chromatography (silica, gradient PE/EA: 8:2 \rightarrow 7:3 \rightarrow 6:4 \rightarrow 5:5) to give compound **9** (180 mg, 57%, 34% overall yield) as a white-beige solid.

$^1\text{H-NMR}$ (400 MHz, CDCl_3) δ 9.38 (s, 1H), 7.89 (d, $J = 1.8$ Hz, 1H), 7.85–7.78 (m, 2H), 7.38–7.17 (m, 8H), 7.10 (t, $J = 6.0$ Hz, 1H), 4.52–4.33 (m, 3H), 1.85 (d, $J = 7.0$ Hz, 3H), 1.47 (s, 9H); $^{13}\text{C-NMR}$ (101 MHz, CDCl_3) δ 169.82, 165.83, 154.73, 141.99, 141.19, 133.45, 133.16, 130.75, 129.32, 127.93, 127.51, 126.34, 126.29, 124.93, 124.03, 123.51, 120.49, 81.41, 44.60, 43.54, 28.40, 22.89; HRFT-MS (ESI+): $m/z = 580.0858$ and 582.0850 (calc. 580.0876 and 582.0856 for $[\text{M} + \text{Na}]^+$).

3.3.26. Synthesis of *N*-[2-amino-5-(thiophen-2-yl)phenyl]-4-[(2-fluoropropanamido)methyl]benzamide (**BA1**)

Compound **4a** (140 mg, 0.28 mmol) was synthesized according to the general procedure **A4** to give after filtration compound **BA1** (53 mg, 53%) as light-brown solid.

UV purity: 98% ($t_{\text{R}} = 8.69$ min); $^1\text{H-NMR}$ (400 MHz, $\text{DMSO-}d_6$) δ 9.70 (s, 1H), 8.84–8.76 (m, 1H), 7.96 (d, $J = 8.2$ Hz, 2H), 7.48 (d, $J = 2.2$ Hz, 1H), 7.39 (d, $J = 8.2$ Hz, 2H), 7.35 (dd, $J = 5.1, 1.2$ Hz, 1H), 7.30 (dd, $J = 8.3, 2.2$ Hz, 1H), 7.24 (dd, $J = 3.6, 1.2$ Hz, 1H), 7.05 (dd, $J = 5.1, 3.6$ Hz, 1H), 6.82 (d, $J = 8.3$ Hz, 1H), 5.19–4.99 (m, 3H), 4.39 (d, $J = 6.1$ Hz, 2H), 1.47 (dd, $J = 24.5, 6.7$ Hz, 3H); $^{19}\text{F-NMR}$ (377 MHz, $\text{DMSO-}d_6$) $\delta -181.06$ (^1H decoupled); $^{13}\text{C-NMR}$ (101 MHz, $\text{DMSO-}d_6$) δ 169.99 (d, $J = 20.2$ Hz), 165.29, 144.23, 142.99, 142.82, 133.07, 128.20, 127.90, 126.90, 123.90, 123.40, 123.21, 122.24, 121.01, 116.36, 87.96 (d, $J = 179.1$ Hz), 41.50, 18.47 (d, $J = 22.0$ Hz); HRFT-MS (ESI+): $m/z = 398.1341$ (calc. 398.1333 for $[\text{M} + \text{H}]^+$).

3.3.27. Synthesis of *N*-[2-amino-5-(thiophen-2-yl)phenyl]-4-(2-fluoropropanamido)benzamide (**BA2**)

Compound **5a** (200 mg, 0.414 mmol) was synthesized according to the general procedure **A4** to give after filtration compound **BA2** (144 mg, 91%) as greyish solid.

UV purity: 99% ($t_{\text{R}} = 8.95$ min); $^1\text{H-NMR}$ (400 MHz, $\text{DMSO-}d_6$) δ 10.34 (s, 1H), 9.67 (s, 1H), 8.03–7.96 (m, 2H), 7.86–7.78 (m, 2H), 7.48 (d, $J = 2.2$ Hz, 1H), 7.35 (dd, $J = 5.1, 1.1$ Hz, 1H), 7.30 (dd, $J = 8.3, 2.2$ Hz, 1H), 7.25 (dd, $J = 3.5, 1.2$ Hz, 1H), 7.05 (dd, $J = 5.1, 3.6$ Hz, 1H), 6.82 (d, $J = 8.3$ Hz, 1H), 5.23 (dq, $J = 48.5, 6.6$ Hz, 1H), 5.14 (s, 2H), 1.55 (dd, $J = 24.6, 6.7$ Hz, 3H); $^{19}\text{F-NMR}$ (377 MHz, DMSO) $\delta -179.76$ (^1H decoupled); $^{13}\text{C-NMR}$ (101 MHz, $\text{DMSO-}d_6$) δ 168.85 (d, $J = 20.6$ Hz), 164.78, 142.59, 141.69, 140.96, 129.69, 128.63, 126.54, 125.75, 124.57, 124.46, 123.89, 123.49, 119.17, 117.65, 116.33, 87.79 (d, $J = 179.0$ Hz), 18.28 (d, $J = 22.2$ Hz); HRFT-MS (ESI+): $m/z = 384.1196$ (calc. 384.1177 for $[\text{M} + \text{H}]^+$).

3.3.28. Synthesis of *N*-[2-amino-5-(thiophen-3-yl)phenyl]-4-[(2-fluoropropanamido)methyl]benzamide (**BA3**)

Compound **4b** (530 mg, 1.06 mmol) was synthesized according to the general procedure **A4** to give after filtration compound **BA3** (244 mg, 58%) as beige solid.

UV purity: 99% ($t_{\text{R}} = 8.60$ min); $^1\text{H-NMR}$ (400 MHz, $\text{DMSO-}d_6$) δ 9.71 (s, 1H), 8.80 (dt, $J = 6.3, 3.3$ Hz, 1H), 7.97 (d, $J = 8.0$ Hz, 2H), 7.60–7.50 (m, 3H), 7.45–7.33 (m, 4H), 6.82 (d, $J = 8.3$ Hz, 1H), 5.20–4.96 (m, 3H), 4.39 (d, $J = 6.1$ Hz, 2H), 1.47 (dd, $J = 24.5, 6.7$ Hz, 3H); $^{19}\text{F-NMR}$ (377 MHz, $\text{DMSO-}d_6$) $\delta -181.06$ (dq, $J = 49.0, 24.5$ Hz); $^{13}\text{C-NMR}$ (101 MHz, $\text{DMSO-}d_6$) δ 169.99 (d, $J = 20.3$ Hz), 165.22, 142.76, 142.55, 141.68, 133.14, 127.86, 126.90, 126.55, 125.74, 124.54, 124.50, 123.88, 123.41, 117.66, 116.32, 87.96 (d, $J = 179.0$ Hz), 41.51, 18.47 (d, $J = 21.9$ Hz); HRFT-MS (ESI+): $m/z = 420.1163$ (calc. 420.1152 for $[\text{M} + \text{Na}]^+$).

3.3.29. Synthesis of *N*-[2-amino-5-(thiophen-3-yl)phenyl]-4-(2-fluoropropanamido)benzamide (**BA4**)

Compound **5b** (100 mg, 0.207 mmol) was synthesized according to the general procedure **A4** to give after filtration compound **BA4** (60 mg, 76%) as light-brown solid.

UV purity: 99% ($t_R = 8.86$ min); $^1\text{H-NMR}$ (400 MHz, $\text{DMSO-}d_6$) δ 10.34 (s, 1H), 9.67 (s, 1H), 8.04–7.97 (m, 2H), 7.87–7.80 (m, 2H), 7.49 (d, $J = 2.2$ Hz, 1H), 7.35 (dd, $J = 5.1, 1.1$ Hz, 1H), 7.30 (dd, $J = 8.3, 2.2$ Hz, 1H), 7.25 (dd, $J = 3.6, 1.2$ Hz, 1H), 7.05 (dd, $J = 5.1, 3.6$ Hz, 1H), 6.82 (d, $J = 8.3$ Hz, 1H), 5.32–5.09 (m, 3H), 1.56 (dd, $J = 24.5, 6.7$ Hz, 3H); $^{19}\text{F-NMR}$ (377 MHz, $\text{DMSO-}d_6$) δ –179.75 (^1H decoupled); $^{13}\text{C-NMR}$ (101 MHz, $\text{DMSO-}d_6$) δ 168.86 (d, $J = 20.5$ Hz), 164.85, 144.25, 143.03, 141.00, 129.62, 128.67, 128.21, 123.92, 123.88, 123.48, 123.20, 122.27, 121.01, 119.18, 116.38, 87.80 (d, $J = 179.1$ Hz), 18.28 (d, $J = 22.1$ Hz); HRFT-MS (ESI+): $m/z = 384.1184$ (calc. 384.1177 for $[\text{M} + \text{H}]^+$).

3.3.30. Synthesis of *N*-(4-amino-4'-fluoro-[1,1'-biphenyl]-3-yl)-4-[(2-fluoropropanamido)methyl]benzamide (**BA5**)

Compound **4c** (255 mg, 0.4 mmol) was synthesized according to the general procedure **A4** to give after filtration compound **BA5** (104 mg, 64%) as white solid.

UV purity: 99% ($t_R = 8.90$ min); $^1\text{H-NMR}$ (400 MHz, $\text{DMSO-}d_6$) δ 9.70 (s, 1H), 8.80 (t, $J = 6.4$ Hz, 1H), 7.96 (d, $J = 7.9$ Hz, 2H), 7.58 (dd, $J = 8.5, 5.4$ Hz, 2H), 7.53–7.46 (m, 1H), 7.39 (d, $J = 7.9$ Hz, 2H), 7.30 (dd, $J = 8.3, 2.3$ Hz, 1H), 7.21 (t, $J = 8.7$ Hz, 2H), 6.86 (d, $J = 8.3$ Hz, 1H), 5.09 (s, 2H), 5.09 (dq, $J = 49.0, 6.7$ Hz, 1H), 4.39 (d, $J = 6.1$ Hz, 2H), 1.47 (dd, $J = 24.5, 6.7$ Hz, 3H); $^{19}\text{F-NMR}$ (377 MHz, $\text{DMSO-}d_6$) δ –117.39––117.60 (m), –181.07 (ddd, $J = 47.4, 28.4, 14.1$ Hz); $^{13}\text{C-NMR}$ (101 MHz, $\text{DMSO-}d_6$) δ 170.00 (d, $J = 20.3$ Hz), 165.30, 161.01 (d, $J = 242.6$ Hz), 142.79, 142.70, 136.75, 133.18, 127.88, 127.30 (d, $J = 7.7$ Hz), 127.16, 126.92, 124.73, 124.63, 123.59, 116.51, 115.50 (d, $J = 21.3$ Hz), 87.97 (d, $J = 179.3$ Hz), 41.51, 18.48 (d, $J = 22.1$ Hz); HRFT-MS (ESI+): $m/z = 410.1704$ (calc. 410.1675 for $[\text{M} + \text{H}]^+$).

3.3.31. Synthesis of *N*-(4-amino-4'-fluoro-[1,1'-biphenyl]-3-yl)-4-(2-fluoropropanamido)benzamide (**BA6**)

Compound **5c** (160 mg, 0.323 mmol) was synthesized according to the general procedure **A4** to give after filtration compound **BA6** (86 mg, 67%) as white solid.

UV purity: 95% ($t_R = 9.15$ min); $^1\text{H-NMR}$ (400 MHz, $\text{DMSO-}d_6$) δ 10.34 (s, 1H), 9.67 (s, 1H), 8.03–7.97 (m, 2H), 7.83 (d, $J = 8.7$ Hz, 2H), 7.61–7.55 (m, 2H), 7.50 (d, $J = 2.2$ Hz, 1H), 7.30 (dd, $J = 8.3, 2.3$ Hz, 1H), 7.25–7.16 (m, 2H), 6.87 (d, $J = 8.4$ Hz, 1H), 5.23 (dq, $J = 48.6, 6.7$ Hz, 1H), 5.09 (s, 2H), 1.55 (dd, $J = 24.5, 6.7$ Hz, 3H); $^{19}\text{F-NMR}$ (377 MHz, $\text{DMSO-}d_6$) δ –117.50 (tt, $J = 9.0, 5.3$ Hz), –179.77 (dq, $J = 48.9, 24.4$ Hz); $^{13}\text{C-NMR}$ (101 MHz, $\text{DMSO-}d_6$) δ 168.85 (d, $J = 20.6$ Hz), 164.84, 161.01 (d, $J = 242.7$ Hz), 142.73, 140.97, 136.73 (d, $J = 3.1$ Hz), 129.71, 128.64, 127.30 (d, $J = 7.9$ Hz), 127.16, 124.76, 124.59, 123.66, 119.18, 116.51, 115.50 (d, $J = 21.2$ Hz), 87.79 (d, $J = 179.1$ Hz), 18.27 (d, $J = 22.2$ Hz); HRFT-MS (ESI+): $m/z = 396.1540$ (calc. 396.1518 for $[\text{M} + \text{H}]^+$).

3.3.32. Synthesis of *N*-[2-amino-5-(furan-2-yl)phenyl]-4-[(2-fluoropropanamido)methyl]benzamide (**BA7**)

Compound **4d** (260 mg, 0.54 mmol) was synthesized according to the general procedure **A4** to give after filtration compound **BA7** (39 mg, 19%) beige solid.

UV purity: 95% ($t_R = 8.41$ min); $^1\text{H-NMR}$ (400 MHz, $\text{DMSO-}d_6$) δ 9.67 (s, 1H), 8.84–8.76 (m, 1H), 7.99–7.93 (m, 2H), 7.60 (dd, $J = 1.9, 0.8$ Hz, 1H), 7.54 (d, $J = 2.0$ Hz, 1H), 7.39 (d, $J = 8.0$ Hz, 2H), 7.33 (dd, $J = 8.3, 2.1$ Hz, 1H), 6.82 (d, $J = 8.4$ Hz, 1H), 6.61 (dd, $J = 3.3, 0.8$ Hz, 1H), 6.51 (dd, $J = 3.4, 1.8$ Hz, 1H), 5.20–4.98 (m, 3H), 4.39 (d, $J = 6.2$ Hz, 2H), 1.47 (dd, $J = 24.5, 6.7$ Hz, 3H); $^{19}\text{F-NMR}$ (377 MHz, $\text{DMSO-}d_6$) δ –181.06 (dq, $J = 49.1, 24.5$ Hz); $^{13}\text{C-NMR}$ (101 MHz, $\text{DMSO-}d_6$) δ 169.99 (d, $J = 20.3$ Hz), 165.31, 153.79, 142.92, 142.79, 141.21, 133.12, 127.88, 126.95, 126.91, 123.24, 122.27, 119.18, 116.18, 111.78, 102.39, 87.96 (d, $J = 179.1$ Hz), 41.51, 18.47 (d, $J = 22.0$ Hz); HRFT-MS (ESI+): $m/z = 382.1563$ (calc. 382.1561 for $[\text{M} + \text{H}]^+$).

3.3.33. Synthesis of *N*-[2-amino-5-(furan-2-yl)phenyl]-4-(2-fluoropropanamido)benzamide (**BA8**)

Compound **5d** (240 mg, 0.513 mmol) was synthesized according to the general procedure **A4** to give after filtration compound **BA8** (29 g, 15%) as orange solid.

UV purity: 95% ($t_R = 8.77$ min); $^1\text{H-NMR}$ (400 MHz, $\text{DMSO-}d_6$) δ 10.35 (s, 1H), 9.65 (s, 1H), 8.03–7.95 (m, 2H), 7.86–7.79 (m, 2H), 7.60 (d, $J = 1.8$ Hz, 1H), 7.53 (d, $J = 2.1$ Hz, 1H), 7.33 (dd, $J = 8.3, 2.1$ Hz, 1H), 6.82 (d, $J = 8.4$ Hz, 1H), 6.61 (d, $J = 3.4$ Hz, 1H), 6.50 (dd, $J = 3.3, 1.8$ Hz, 1H), 5.34–5.09 (m, 3H), 1.55 (dd, $J = 24.6, 6.7$ Hz, 3H); $^{19}\text{F-NMR}$ (377 MHz, $\text{DMSO-}d_6$) δ –179.78 (dq, $J = 48.9, 24.6$ Hz); $^{13}\text{C-NMR}$ (101 MHz, $\text{DMSO-}d_6$) δ 168.84 (d, $J = 20.5$ Hz), 164.86, 153.80, 142.94, 141.19, 140.98, 129.66, 128.63, 123.33, 122.30, 122.20, 119.20, 119.16, 116.19, 111.78, 102.38, 87.77 (d, $J = 179.1$ Hz), 18.27 (d, $J = 22.2$ Hz); HRFT-MS (ESI+): $m/z = 368.1408$ (calc. 368.1405 for $[\text{M}+\text{H}]^+$).

3.3.34. Synthesis of *N*-[2-amino-5-(furan-3-yl)phenyl]-4-[(2-fluoropropanamido)methyl]benzamide (**BA9**)

Compound **4e** (234 mg, 0.486 mmol) was synthesized according to the general procedure **A4** to give after filtration compound **BA9** (50 mg, 27%) as beige solid.

UV purity: 96% ($t_R = 8.24$ min); $^1\text{H-NMR}$ (400 MHz, $\text{DMSO-}d_6$) δ 9.70 (s, 1H), 8.84–8.76 (m, 1H), 8.00–7.93 (m, 3H), 7.66 (t, $J = 1.7$ Hz, 1H), 7.42–7.35 (m, 3H), 7.24 (dd, $J = 8.3, 2.1$ Hz, 1H), 6.86–6.77 (m, 2H), 5.09 (dq, $J = 48.9, 6.7$ Hz, 1H), 4.97 (s, 2H), 4.39 (d, $J = 6.1$ Hz, 2H), 1.47 (dd, $J = 24.5, 6.7$ Hz, 3H); $^{19}\text{F-NMR}$ (377 MHz, $\text{DMSO-}d_6$) δ –181.05 (dq, $J = 49.0, 24.5$ Hz); $^{13}\text{C-NMR}$ (101 MHz, $\text{DMSO-}d_6$) δ 170.00 (d, $J = 20.1$ Hz), 165.19, 143.82, 142.76, 142.42, 137.34, 133.10, 127.84, 126.90, 125.93, 124.15, 124.09, 123.46, 120.22, 116.34, 108.53, 87.96 (d, $J = 179.1$ Hz), 41.50, 18.47 (d, $J = 21.9$ Hz); HRFT-MS (ESI+): $m/z = 382.1564$ (calc. 382.1561 for $[\text{M}+\text{H}]^+$).

3.3.35. Synthesis of *N*-[2-amino-5-(furan-3-yl)phenyl]-4-(2-fluoropropanamido)benzamide (**BA10**)

Compound **5e** (150 g, 0.32 mmol) was synthesized according to the general procedure **A4** to give after filtration compound **BA10** (104 mg, 88%) as light-brown solid.

UV purity: 96% ($t_R = 8.49$ min); $^1\text{H-NMR}$ (400 MHz, $\text{DMSO-}d_6$) δ 10.35 (s, 1H), 9.68 (s, 1H), 8.04–7.94 (m, 3H), 7.87–7.78 (m, 2H), 7.66 (t, $J = 1.7$ Hz, 1H), 7.40 (d, $J = 2.1$ Hz, 1H), 7.24 (dd, $J = 8.2, 2.1$ Hz, 1H), 6.84–6.77 (m, 2H), 5.23 (dq, $J = 48.5, 6.7$ Hz, 1H), 4.98 (s, 2H), 1.56 (dd, $J = 24.5, 6.7$ Hz, 3H); $^{19}\text{F-NMR}$ (377 MHz, $\text{DMSO-}d_6$) δ –179.77 (^1H decoupled); $^{13}\text{C-NMR}$ (101 MHz, $\text{DMSO-}d_6$) δ 168.86 (d, $J = 20.7$ Hz), 164.75, 143.82, 142.47, 140.97, 137.35, 129.65, 128.62, 125.95, 124.20, 124.06, 123.54, 120.24, 119.17, 116.35, 108.54, 87.79 (d, $J = 179.0$ Hz), 18.28 (d, $J = 22.1$ Hz); HRFT-MS (ESI+): $m/z = 368.1416$ (calc. 368.1405 for $[\text{M}+\text{H}]^+$).

3.4. Radiosynthesis

3.4.1. Manual Radiosynthesis of [^{18}F]BA3

No-carrier-added (n.c.a.) [^{18}F]fluoride was produced via the $^{18}\text{O}(\text{p},\text{n})^{18}\text{F}$ nuclear reaction by irradiation of the conical shaped [^{18}O]H₂O (Hyox 18 enriched water; Rotem Industries Ltd., Mishor Yamin, Israel) target Nirta[®] Conical 5 (IBA RadioPharma Solutions, Louvain-la-Neuve, Belgium) on a Cyclone 18/9 (IBA RadioPharma Solutions, Louvain-la-Neuve, Belgium) with 18 MeV proton beam or [^{18}O]H₂O recycled by the established in-house method [66]. [^{18}F]Fluoride in 1.5 mL of H₂O was trapped on a Sep-Pak[®] Accell QMA light cartridge (sorbent weight: 46 mg; preconditioned with 10 mL of an aqueous 0.5 M NaHCO₃ solution and 10 mL water, Waters, Milford, MA, USA). The activity was eluted with 390 μL of an aqueous solution of K₂CO₃ (1.8 mg, 13 μmol), KHCO₃ (1.35 mg, 13 μmol) or K₂C₂O₄ (1.84 mg, 10 μmol), respectively, into a 5 mL microwave V-vial (CEM[®] Corporation, Matthews, NC, USA) and K_{2.2.2} (11 mg, 29 μmol) or 18-crown-6 (10 mg, 38 μmol), respectively, in 1 mL of MeCN was added. For investigations of the precursor to base ratio, the amount of potassium carbonate was accordingly reduced or increased.

For labelling with [^{18}F]TBAF, the tetra-*n*-butylammonium hydrogen carbonate (TBAHCO₃) solution (150 μL , 0.075 M, ABX, Radeberg, Germany) was directly placed into the V-vial containing [^{18}F]fluoride and 1 mL of MeCN. The solution was azeotropically dried under vacuum and argon flow in the microwave cavity (Discover PETwave microwave CEM[®] corporation, 50–60 $^{\circ}\text{C}$, 75 W) for 8–10 min. Additional aliquots of MeCN (2; \times , 10mL), were added during the drying process and the final complex was dissolved in an appropriate volume of labelling solvent and used directly or divided in several portions. Thereafter, a solution containing the bromo precursor **9** (2–3 mg, 3.6–5.4 μmol) in 300 μL of an appropriate solvent was added, and ^{18}F -labelling was performed at different temperatures in dependence of the solvent used (80, 100 and 150 $^{\circ}\text{C}$). The reaction was monitored in different time points (up to 20 min) via radio-thin layer chromatography (radio-TLC) and (radio-)reversed phase high-performance liquid chromatography ((radio)-RP-HPLC, see quality control).

3.4.2. Automated Radiosynthesis of [^{18}F]BA3

Remotely controlled radiosynthesis was performed using a TRACERlab FX2 N synthesizer (GE Healthcare, Waukesha, WI, USA) equipped with a Laboport vacuum pump N810.3FT.18 (KNF Neuberger GmbH, Freiburg, Germany), a BlueShadow UV detector 10D (KNAUER GmbH, Berlin, Germany) and the TRACERlab FX Software (Version 2.3.0, GE Healthcare, Waukesha, WI, USA) with the optimized radiolabelling conditions. [^{18}F]TBAF complex was obtained after trapping [^{18}F]fluoride (7–32 GBq) on a Sep-Pak[®] Accell QMA light cartridge (Figure S1, entry 1, sorbent weight: 46 mg; preconditioned with 10 mL of an aqueous 0.5 M NaHCO₃ solution and 10 mL water, Waters, Milford, MA, USA) and eluted into the reactor with a solution of 150 μL of TBAHCO₃ (entry 2, 0.075 M ABX GmbH, Radeberg, Germany), 300 μL of H₂O and 600 μL of MeCN. After azeotropic drying at 50 $^{\circ}\text{C}$ for 3 min, 2 mL MeCN (entry 3) were added and azeotropic drying was continued for further 3 min at 70 $^{\circ}\text{C}$ and 1 min at 40 $^{\circ}\text{C}$. Thereafter, the nucleophilic aliphatic radiofluorination proceeded by adding the bromo precursor **9** (4 mg, 7.2 μmol) dissolved in 800 μL of MeCN (entry 4) and stirring the reaction mixture at 100 $^{\circ}\text{C}$ for 15 min. The reaction mixture was cooled to 40 $^{\circ}\text{C}$ and the Boc deprotection was carried out by adding 800 μL of a 2 M HCl_{aq} solution (entry 5) and subsequent heating at 80 $^{\circ}\text{C}$ for another 5 min. After neutralization with a mixture of 1.6 mL of an aqueous 1 M NaHCO₃ solution and 1.8 mL of 100 mM aqueous phosphate buffer (pH = 6, entry 6), the solution was transferred into the injection vial (entry 7). [^{18}F]BA3 was isolated by semipreparative RP-HPLC (column: Reprosil-Pur C18-AQ, 250 \times 10 mm, 10 μm ; Dr. Maisch HPLC GmbH, Ammerbuch, Germany) with a solvent composition of 40% MeCN/20 mM NH₄OAc_{aq} at a flow rate of 4.0 mL/min (entry 8). The radiotracer [^{18}F]BA3 was collected in the HPLC collection vial containing 40 mL of H₂O (entry 9), trapped on a Sep-Pak[®] C18 light cartridge (entry 10, sorbent weight: 130 mg; preconditioned with 5 mL EtOH and 10 mL water, Waters, Milford, MA, USA) and followed by washing with 2 mL of H₂O (entry 11) and elution of [^{18}F]BA3 with 1.3 mL EtOH (entry 12) in the product vial (entry 13). The ethanolic solution was transferred outside of the hotcell by remote control, the solvent was reduced manually in a stream of argon at 70 $^{\circ}\text{C}$ and the desired radiotracer was reconstituted in a saline solution (NaCl 0.9%) containing max. 10% EtOH (*v/v*). [^{18}F]BA3 was then ready for further biological characterization in a total synthesis time of about 85 min.

3.4.3. Quality Control and Analyses

Radio-thin layer chromatography (radio-TLC) of [^{18}F]BA3 was performed on Alugram[®] SIL G/UV254 pre-coated plates (Macherey-Nagel, Düren, Germany) with DCM/MeOH (4:1, *v/v*). The plates were exposed to storage phosphor screens (BAS IP MS 2025 E, GE Healthcare Europe GmbH, Freiburg, Germany) and recorded using the Amersham Typhoon RGB Biomolecular Imager (GE Healthcare Life Sciences, Freiburg, Germany). Images were quantified with the ImageQuant TL8.1 software (Version 8.1, GE Healthcare Life Sciences, Freiburg, Germany). Analytical chromatographic separations were performed on

a JASCO LC-2000 system, incorporating a PU-2080Plus pump, AS-2055Plus auto injector (100 μ L sample loop), and a UV-2070Plus detector (JASCO Deutschland GmbH, Pfungstadt, Germany) coupled with a gamma radioactivity HPLC flow detector (Gabi Star, raytest Isotopenmessgeräte GmbH, Straubenhardt, Germany). Data analysis was performed with the Galaxie chromatography software (Agilent Technologies, Santa Clara, CA, USA) using the chromatograms obtained at 254 nm. Radiochemical yield from aliquots of the reaction mixture, radiochemical purities and in vivo metabolism analysis of plasma, brain and urine samples were assessed via reverse phase—high performance liquid chromatography (RP-HPLC) with a Reprosil-Pur C18-AQ column (250 \times 4.6 mm, 5 μ m) in gradient mode (0–5 min: 10% MeCN/20 mM $\text{NH}_4\text{OAc}_{\text{aq}}$, 5–25 min: 10% \rightarrow 90% MeCN/20 mM $\text{NH}_4\text{OAc}_{\text{aq}}$, 25–29 min: 90% MeCN/20 mM $\text{NH}_4\text{OAc}_{\text{aq}}$, 29–30 min: 90% \rightarrow 10% MeCN/20 mM $\text{NH}_4\text{OAc}_{\text{aq}}$, 30–35 min: 10% MeCN/20 mM $\text{NH}_4\text{OAc}_{\text{aq}}$) and a flow of 1.0 mL/min.

The molar activity was determined using analytical RP-HPLC with a Reprosil-Pur C18-AQ column (250 \times 4.6 mm, 5 μ m) and 38% MeCN/20 mM $\text{NH}_4\text{OAc}_{\text{aq}}$ as eluent at a flow rate of 1.0 mL/min obtained at 254 nm.

The ammonium acetate concentrations stated as 20 mM $\text{NH}_4\text{OAc}_{\text{aq}}$ correspond to the concentration in the aqueous component of an eluent mixture.

3.4.4. Determination of Radiochemical Stability and Lipophilicity ($\log D_{7.4}$)

Radiochemical stability of [^{18}F]BA3 was investigated in 0.9% NaCl solution (containing 10% EtOH) and in *n*-octanol at room temperature for 2 h. Samples were analysed by radio-RP-HPLC (see quality control). The $\log D_{7.4}$ value of [^{18}F]BA3 was experimentally determined in *n*-octanol/phosphate-buffered saline (PBS, pH = 7.4) at room temperature by the shake-flask method as described previously [67]. Briefly, small tracer amounts (~800 kBq) were added to a mixture of 3 mL *n*-octanol and 3 mL PBS. After shaking for 20 min, the samples were centrifuged (10,000 rpm, 5 min) and 1 mL aliquots of the organic as well as aqueous layer were taken and measured in a gamma counter (1480 WIZARD, Perkin Elmer, Turku, Finland). Another 1 mL aliquot of the organic layer was mixed with 2 mL *n*-octanol and 3 mL PBS and subjected to the same procedure until constant partition coefficient values had been obtained. The measurement was performed twice in quadruplicate.

3.4.5. Inhibition Assay for HDAC1-3 and HDAC6

In vitro inhibitory activities against HDAC1–3 and HDAC6 were measured as previously published [68] with minor modifications. In short, 3-fold serial dilutions of test compounds and controls in assay buffer (50 mM Tris-HCl, pH = 8.0, 137 mM NaCl, 2.7 mM KCl, 1.0 mM $\text{MgCl}_2 \times 6 \text{H}_2\text{O}$, 0.1 mg/mL BSA) were prepared, and 5.0 μ L were transferred into black microplates (OptiPlate-96, PerkinElmer Inc., Waltham, MA, USA). 25 μ L of assay buffer and 10 μ L enzyme solution (human recombinant HDAC1 (BPS Bioscience Inc., San Diego, CA, USA, Catalog# 50051); HDAC2 (BPS Bioscience Inc., San Diego, CA, USA, Catalog# 50052); HDAC3/NcoR2 (BPS Bioscience Inc., San Diego, CA, USA, Catalog# 50003); HDAC6 (BPS Bioscience Inc., San Diego, CA, USA, Catalog# 50006) were added. Enzyme and inhibitor were preincubated at 25 $^\circ\text{C}$ for 60 min (HDAC1-3) or 15 min (HDAC6). Afterwards, the fluorogenic substrate Z-Lys(Ac)-AMC (ZMAL) [69] (10 μ L; 75 μM in assay buffer) was added. The total assay volume of 50 μ L (max. 1% DMSO) was incubated at 37 $^\circ\text{C}$ for 90 min. Subsequently, 50 μ L trypsin solution (0.4 mg/mL trypsin in buffer: 50 mM Tris-HCl, pH = 8.0, 100 mM NaCl) was added, followed by additional 30 min of incubation at 37 $^\circ\text{C}$. Fluorescence (excitation: 355 nm, emission: 460 nm) was measured using a Thermo ScientificTM Ascent FluoroskanTM microplate reader (Thermo Fisher Scientific, Waltham, MA, USA). All compounds were tested at least twice in duplicates. The 50% inhibitory concentration (IC_{50}) was determined by plotting the dose response curves and nonlinear regression with GraphPad Prism (GraphPad Prism 9.3 for MacOS, GraphPad Software, LLC., San Diego, CA, USA).

3.5. Biological Experiments

All experimental work including animals has been conducted in accordance with the national legislation on the use of animals for research (Tierschutzgesetz [TierSchG], Tierschutz-Versuchstierverordnung [TierSchVersV]) and were approved by the responsible authorities of Saxony (Landesdirektion Sachsen, Referat 25—Veterinärwesen und Lebensmittelüberwachung; TVV 18/18, DD24.1-5131/446/19, valid until 23 June 2023). CD-1 mice (female, 8–15 weeks, 29–43 g) were obtained from the Medizinisch-Experimentelles Zentrum at the Medical Faculty of the Leipzig University (Leipzig, Germany).

3.5.1. Metabolite Analysis

The radiotracer [^{18}F]BA3 (~30 MBq in 200 μL isotonic saline) was administered via the tail vein in non-anesthetized female CD-1 mice ($n = 2$). At 30 min p.i., the animals were anesthetized by isoflurane inhalation and blood was sampled from the retro-orbital plexus. After cervical dislocation, urine was obtained and the brain was isolated. Plasma was obtained by centrifugation of the blood sample ($8000 \times g$, 2 min), and the brain was homogenized in ~1 mL distilled water on ice using a glass/PTFE Potter Homogenizer (Potter S Homogenizer, B. Braun Melsungen AG, Melsungen, Germany).

Protein precipitation was performed by addition of an ice-cold MeCN/ H_2O mixture (9:1, v/v) in a ratio of 4:1 (v/v) of organic solvent to plasma or brain homogenate, respectively. The samples were vortexed for 3 min, equilibrated on ice for 3 min, and centrifuged for 10 min at 10,000 rpm. The precipitates were washed with 100 μL of the solvent mixture and subjected to the same procedure. The combined supernatants were concentrated at 70 $^\circ\text{C}$ under argon flow to a final volume of approximately 100 μL and analysed by analytical radio-RP-HPLC with a gradient system (see quality control section). The peak corresponding to the radiotracer in the radio-chromatogram was identified by co-injecting the sample with the reference compound BA3. To determine the percentage of activity in the supernatants compared with total activity, aliquots of each step as well as the precipitates were quantified by an automated gamma counter (1480 WIZARD, Perkin Elmer, Turku, Finland). For plasma and brain samples recoveries of 97% and 95%, respectively, of total activity were obtained.

For the preparation of the MLC samples, 20 μL of mouse plasma was dissolved in 200 μL of an aqueous 200 mM sodium dodecyl sulfate (SDS_{aq}) solution and injected into the MLC system. For brain samples, 400 μL brain homogenate was dissolved in 800 μL 200 mM SDS_{aq} , heated for 5 min at 70 $^\circ\text{C}$ and centrifuged for 5 min at 10,000 rpm. The MLC system was built up as earlier described [61]. Separations were performed by using a Reprosil-Pur C18-AQ column (250 \times 4.6 mm, 10 μm + 10 mm pre-column) and an eluent mixture of EtOH/100 mM SDS_{aq} /25 mM $(\text{NH}_4)_2\text{HPO}_4$ in gradient mode (0–10 min at 100% 100 mM SDS_{aq} , 10–15 min up to 10% EtOH, 15–20 min at 10% EtOH, 20–21 min up to 100% 100 mM SDS_{aq} ; 21–30 min at 100% 100 mM SDS_{aq}) at a flow rate of 1.0 mL/min.

The sodium dodecyl sulfate concentrations stated as 100 mM SDS_{aq} correspond to the concentration in the aqueous component of an eluent mixture.

3.5.2. Cell Culture

F98 cells (obtained from ATCC[®] Washington, DC, USA) and U251-MG cells (obtained from Drs A. Feldmann and N. Metwasi, Department of Radioimmunology, HZDR, Rossendorf, Germany) were cultivated in Dulbecco's Modified Eagle Medium (DMEM, Gibco, Invitrogen, Dun Laoghaire, Ireland) supplemented with 10% heat inactivated fetal bovine serum (Gibco, Invitrogen, Dun Laoghaire, Ireland), and 100 U/mL penicillin and 100 $\mu\text{g}/\text{mL}$ streptomycin (Gibco, Invitrogen, Dun Laoghaire, Ireland) in a humidified atmosphere in a CO_2 incubator (37 $^\circ\text{C}$, 5% CO_2).

3.5.3. Immunofluorescence Staining

Cells were seeded at 5×10^4 /well in an 8 well micro-slide (Ibidi GmbH, Gräfel-ling, Germany) 48 h before staining. Cells were fixed in 2% PFA (paraformaldehyde) for

20 min at room temperature and then washed twice with PBS. After a 45 min permeabilization/blocking step (0.3 Triton X 100, 5% normal goat serum in PBS), the detection of the HDAC1 was performed by overnight incubation at 4 °C of the slides with the primary rabbit polyclonal antibody (1:500 in blocking buffer 5% normal goat serum, GTX100513, Biozol Diagnostica Vertrieb GmbH, Eching, Germany). After washing with a solution of 1% BSA (bovine serum albumin) in PBS, the slides were incubated for 1 h at room temperature with the goat polyclonal secondary antibody to rabbit IgG (1:200 in dilution buffer 1% BSA, Alexa Fluor® 488; ab150081, Abcam, Berlin, Germany). To finish, cells nuclei were counterstained with Hoechst, 10 min at room temperature (1:1000 in PBS, Hoechst 33258, Life Technologies, Carlsbad, CA, USA). After a step of washing and drying, slides were covered up with mounting medium (Aquapolymount, Polysciences Europe GmbH, Hirschberg an der Bergstrasse, Germany) for observation by fluorescence microscopy (Leica, DMi8, software Leica LASX, Leica Mikrosysteme Vertrieb GmbH, Wetzlar, Germany).

3.5.4. MTS Assay

Proliferation of F98 and U251-MG cells was determined using a commercially available MTS assay (CellTiter 96® Aqueous One Solution Cell Proliferation Assay, Promega GmbH, Walldorf, Germany). Briefly, the cells were seeded into 96-well plates at a density of 5×10^4 cells/well 24 h prior to the experiment at 37 °C in a humidified, 5% CO₂ atmosphere. On the day of the experiment, the cell culture medium was replaced by fresh medium supplemented with either test compounds (working concentration: 50 µM; prepared by 1:200 dilution from a 10 mM stock solution in 100% DMSO with cell culture medium) or vehicle (0.5% DMSO in cell culture medium), and the cells were incubated for 72 h. Subsequently, 20 µL of the MTS solution was added per well and the plate was incubated in the CO₂ incubator for another 2 h. Afterwards, the absorbance was measured at a wavelength of 490 nm using a microplate reader (Model 680 microplate reader, Bio-Rad Laboratories GmbH, Feldkirchen, Germany).

3.5.5. PET Studies

For the time of the experiments, female CD-1 mice ($n = 6$; 8–15 weeks; 29–43 g) were kept in a dedicated climatic chamber with free access to water and food under a 12:12 h dark:light cycle at a constant temperature (24 °C). The animals were anaesthetized (Anaesthesia Unit U-410, agntho's, Lidingö, Sweden) with isoflurane (2.0%, 300 mL/min) delivered in a 60% oxygen/40% air mixture (Gas Blender 100 Series, MCQ instruments, Rome, Italy) and their body temperature maintained at 37 °C with a thermal bed system. For baseline studies [¹⁸F]BA3 was injected into the tail vein ($n = 2$; 6.0 ± 0.6 MBq in 150 µL isotonic saline; 9.2 ± 0.7 nmol/kg; A_m : 21 GBq/µmol, EOS) followed by a dynamic 60 min PET/MR scan (Mediso nanoScan®, Budapest, Hungary). Permeability-glycoprotein efflux transporter studies consisted in pre-treatment via i.v. injection of cyclosporine A (50 mg/kg in NaCl/DMSO/kolliphor, 7:1:2, *v/v*; $n = 2$) or of vehicle (NaCl/DMSO/kolliphor, 7:1:2, *v/v*; $n = 2$) 30 min prior to [¹⁸F]BA3 (6.0 ± 0.9 MBq; 4.9 ± 0.7 nmol/kg; A_m : 32–37 GBq/µmol, EOS). Each PET image was corrected for random coincidences, dead time, scatter and attenuation (AC), based on a whole body (WB) MR scan. The reconstruction parameters for the list mode data were 3D-ordered subset expectation maximization (OSEM), 4 iterations, 6 subsets, energy window: 400–600 keV, coincidence mode: 1–5, ring difference: 81. The mice were positioned prone in a special mouse bed (heated up to 37 °C), with the head fixed to a mouth piece for the anaesthetic gas supply with isoflurane in 40% air and 60% oxygen. The PET data were collected by a continuous WB scan during the entire investigation. Following the 60 min PET scan a T1 weighted WB gradient echo sequence (TR/TE: 20/6.4 ms, NEX: 1, FA: 25, FOV: 64 × 64 mm, Matrix: 128 × 128, STh: 0.5 mm) was performed for AC and anatomical orientation. Image registration and evaluation of the region of interest (ROI) was carried out with PMOD (PMOD Technologies LLC, v. 3.9, Zurich, Switzerland). The respective brain regions were identified using the mouse

brain atlas template Ma-Benveniste-Mirrione-FDG. The activity data are expressed as mean SUV of the overall ROI.

4. Conclusions

A series of novel fluorinated benzamide-based HDAC inhibitors with high inhibition potency and specificity to HDAC1 and HDAC2 was synthesized. With IC_{50} values in the low nanomolar range against HDAC1 (4.8 nM each) and HDAC2 (64.3 and 39.9 nM, respectively), the inhibitors **BA1** and **BA3** emerged as the most promising compounds of the series. **BA3**, the most potent inhibitor of HDAC1 and HDAC2 was subsequently selected for radiofluorination. After optimizing the radiolabelling conditions, a two-step one-pot automated radiosynthesis of [^{18}F]**BA3** using the [^{18}F]TBAF-complex and the TRACERlab FX2 N radiosynthesizer was successfully established. [^{18}F]**BA3** was finally obtained in a low radiochemical yield, but with a high radiochemical purity and good molar activities. The biological evaluation in mice revealed a low brain uptake along with a high amount of radiometabolites of [^{18}F]**BA3** in the brain. These results led to the conclusion that the radiotracer [^{18}F]**BA3** is not suitable for imaging HDAC1/2 in the brain. However, the pharmacological potency of **BA3** in vitro is comparable to that of HDAC inhibitors possessing clinical efficacy in the treatment of cancer diseases, making **BA3** a potential lead structure for the development of new HDAC inhibitors. Consequently, the scaffold of **BA3** requires further modifications to optimize properties such as the metabolic stability and the brain penetration.

Supplementary Materials: The following are available online at <https://www.mdpi.com/article/10.3390/ph15030324/s1>, Figure S1: Scheme of the synthesis module TRACERlab FX2 N for the radiosynthesis of [^{18}F]**BA3**; Figure S2: Representative (A) UV- and (B) radio-RP-HPLC chromatograms of formulated [^{18}F]**BA3**, Figure S3: Representative radio-MLC chromatograms of in vivo metabolism studies, Figure S4: Baseline time–activity curves (TACs) of CD-1 mice brain region after injection of [^{18}F]**BA3**, Figure S5: Biodistribution of [^{18}F]**BA3** at different time points derived from PET imaging, Figure S6: Representative maximal intensity projection map of [^{18}F]**BA3**, Figures S7–S46: 1H -, ^{13}C - and ^{19}F -NMR spectra and LC-MS chromatograms for compounds **BA1–BA10**, Table S1: Tissue biodistribution of radioactivity at different time point after i.v. injection of [^{18}F]**BA3** in CD-1 mice.

Author Contributions: Conceptualization, O.C., B.W., W.D.-C., P.B., F.K.H. and M.S.; methodology, O.C., L.S.-H., B.W., M.T., W.D.-C., F.-A.L., F.K.H. and M.S.; investigation, O.C., L.S.-H., B.W., M.T., W.D.-C., D.G., R.T., S.D.-S. and M.S.; writing—original draft preparation, O.C.; writing—review and editing, L.S.-H., B.W., M.T., W.D.-C., D.G., R.T., S.D.-S., F.-A.L., K.K., P.B., F.K.H. and M.S.; visualization, O.C., L.S.-H., B.W., M.T., W.D.-C., D.G., R.T., S.D.-S., F.-A.L., K.K., P.B., F.K.H. and M.S.; supervision, B.W., W.D.-C., K.K., P.B. and M.S.; project administration, O.C., P.B., F.K.H. and M.S. All authors have read and agreed to the published version of the manuscript.

Funding: The work of O.C. was funded by a stipend of the European Social Fund (ESF, grant 100343060).

Institutional Review Board Statement: All experimental work including animals has been conducted in accordance with the national legislation on the use of animals for research (Tierschutzgesetz [TierSchG], Tierschutz-Versuchstierverordnung [TierSchVersV]) and were approved by the responsible authorities of Saxony (Landesdirektion Sachsen, Referat 25—Veterinärwesen und Lebensmittelüberwachung; TVV 18/18, DD24.1-5131/446/19, valid until 23 June 2023).

Informed Consent Statement: Not applicable.

Data Availability Statement: Data is contained within the article or Supplementary Materials.

Acknowledgments: We thank Maik Icker and the staff of the MS Core Facility, Department of Chemistry and Mineralogy of University Leipzig (Leipzig, Germany), for NMR and HRFT-MS measurements, Karsten Franke and Steffen Fischer, Helmholtz-Zentrum Dresden-Rossendorf (HZDR), for providing [^{18}F]fluoride and Tina Spalholz, HZDR, for technical assistance.

Conflicts of Interest: The authors declare no conflict of interest.

References

1. Tago, T.; Toyohara, J. Advances in the Development of PET Ligands Targeting Histone Deacetylases for the Assessment of Neurodegenerative Diseases. *Molecules* **2018**, *23*, 300. [[CrossRef](#)] [[PubMed](#)]
2. Lane, A.A.; Chabner, B.A. Histone deacetylase inhibitors in cancer therapy. *J. Clin. Oncol.* **2009**, *27*, 5459–5468. [[CrossRef](#)] [[PubMed](#)]
3. Chuang, D.M.; Leng, Y.; Marinova, Z.; Kim, H.J.; Chiu, C.T. Multiple roles of HDAC inhibition in neurodegenerative conditions. *Trends Neurosci.* **2009**, *32*, 591–601. [[CrossRef](#)]
4. West, A.C.; Johnstone, R.W. New and emerging HDAC inhibitors for cancer treatment. *J. Clin. Investig.* **2014**, *124*, 30–39. [[CrossRef](#)] [[PubMed](#)]
5. Chen, H.P.; Zhao, Y.T.; Zhao, T.C. Histone deacetylases and mechanisms of regulation of gene expression. *Crit. Rev. Oncog.* **2015**, *20*, 35–47. [[CrossRef](#)]
6. Wang, D.F.; Helquist, P.; Wiech, N.L.; Wiest, O. Toward selective histone deacetylase inhibitor design: Homology modeling, docking studies, and molecular dynamics simulations of human class I histone deacetylases. *J. Med. Chem.* **2005**, *48*, 6936–6947. [[CrossRef](#)]
7. Ho, T.C.S.; Chan, A.H.Y.; Ganesan, A. Thirty Years of HDAC Inhibitors: 2020 Insight and Hindsight. *J. Med. Chem.* **2020**, *63*, 12460–12484. [[CrossRef](#)]
8. Li, G.; Tian, Y.; Zhu, W.G. The Roles of Histone Deacetylases and Their Inhibitors in Cancer Therapy. *Front. Cell Dev. Biol.* **2020**, *8*, 576946. [[CrossRef](#)]
9. Turnbull, R.E.; Fairall, L.; Saleh, A.; Kelsall, E.; Morris, K.L.; Ragan, T.J.; Savva, C.G.; Chandru, A.; Millard, C.J.; Makarova, O.V.; et al. The MiDAC histone deacetylase complex is essential for embryonic development and has a unique multivalent structure. *Nat. Commun.* **2020**, *11*, 3252. [[CrossRef](#)]
10. Witt, O.; Deubzer, H.E.; Milde, T.; Oehme, I. HDAC family: What are the cancer relevant targets? *Cancer Lett.* **2009**, *277*, 8–21. [[CrossRef](#)]
11. Wang, X.Q.; Bai, H.M.; Li, S.T.; Sun, H.; Min, L.Z.; Tao, B.B.; Zhong, J.; Li, B. Knockdown of HDAC1 expression suppresses invasion and induces apoptosis in glioma cells. *Oncotarget* **2017**, *8*, 48027–48040. [[CrossRef](#)] [[PubMed](#)]
12. Lee, D.H.; Ryu, H.W.; Won, H.R.; Kwon, S.H. Advances in epigenetic glioblastoma therapy. *Oncotarget* **2017**, *8*, 18577–18589. [[CrossRef](#)] [[PubMed](#)]
13. Shukla, S.; Tekwani, B.L. Histone Deacetylases Inhibitors in Neurodegenerative Diseases, Neuroprotection and Neuronal Differentiation. *Front. Pharmacol.* **2020**, *11*, 537. [[CrossRef](#)] [[PubMed](#)]
14. Jenke, R.; Rensing, N.; Hansen, F.K.; Aigner, A.; Buch, T. Anticancer Therapy with HDAC Inhibitors: Mechanism-Based Combination Strategies and Future Perspectives. *Cancers* **2021**, *13*, 634. [[CrossRef](#)]
15. Kunadis, E.; Lakiotaki, E.; Korkolopoulou, P.; Piperi, C. Targeting post-translational histone modifying enzymes in glioblastoma. *Pharmacol. Ther.* **2021**, *220*, 107721. [[CrossRef](#)]
16. Camphausen, K.; Burgan, W.; Cerra, M.; Oswald, K.A.; Trepel, J.B.; Lee, M.J.; Tofilon, P.J. Enhanced radiation-induced cell killing and prolongation of gammaH2AX foci expression by the histone deacetylase inhibitor MS-275. *Cancer Res.* **2004**, *64*, 316–321. [[CrossRef](#)]
17. Camphausen, K.; Scott, T.; Sproull, M.; Tofilon, P.J. Enhancement of xenograft tumor radiosensitivity by the histone deacetylase inhibitor MS-275 and correlation with histone hyperacetylation. *Clin. Cancer Res.* **2004**, *10*, 6066–6071. [[CrossRef](#)]
18. Diss, E.; Nalobothula, N.; Nguyen, D.M.; Chang, E.T.; Kwok, Y.; Carrier, F. Vorinostat/SAHA Promotes Hyper-Radiosensitivity in Wild Type p53 Human Glioblastoma Cells. *JSM Clin. Oncol. Res.* **2014**, *2*, 1004.
19. Hendricks, J.A.; Keliher, E.J.; Marinelli, B.; Reiner, T.; Weissleder, R.; Mazitschek, R. In vivo PET imaging of histone deacetylases by 18F-suberoylanilide hydroxamic acid (18F-SAHA). *J. Med. Chem.* **2011**, *54*, 5576–5582. [[CrossRef](#)]
20. Mukhopadhyay, U.; Tong, W.P.; Gelovani, J.G.; Alauddin, M.M. Radiosynthesis of 6-([18F]fluoroacetamido)-1-hexanoic anilide ([18F]FAHA) for PET imaging of histone deacetylase (HDAC). *J. Label. Compd. Radiopharm.* **2006**, *49*, 997–1006. [[CrossRef](#)]
21. Reid, A.E.; Hooker, J.; Shumay, E.; Logan, J.; Shea, C.; Kim, S.W.; Collins, S.; Xu, Y.; Volkow, N.; Fowler, J.S. Evaluation of 6-([18F]fluoroacetamido)-1-hexanoic anilide for PET imaging of histone deacetylase in the baboon brain. *Nucl. Med. Biol.* **2009**, *36*, 247–258. [[CrossRef](#)] [[PubMed](#)]
22. Yeh, H.H.; Tian, M.; Hinz, R.; Young, D.; Shavrin, A.; Mukhopadhyay, U.; Flores, L.G.; Balatoni, J.; Soghomonyan, S.; Jeong, H.J.; et al. Imaging epigenetic regulation by histone deacetylases in the brain using PET/MRI with 18F-FAHA. *Neuroimage* **2013**, *64*, 630–639. [[CrossRef](#)] [[PubMed](#)]
23. Li, F.; Cho, S.J.; Yu, L.; Hudson, R.H.; Luyt, L.; Pin, C.; Kovacs, M.; Koropatnick, J.; Lee, T.-Y. Evaluation of 6-([18F]fluoroacetamido)-1-hexanoic-anilide (18F-FAHA) as imaging probe in tumor xenograft mice model. *SPIE Med. Imaging* **2016**, *9788*, 978814. [[CrossRef](#)]
24. Fukumitsu, N.; Yeh, S.H.; Flores, L.G.; Mukhopadhyay, U.; Young, D.; Ogawa, K.; Jeong, H.J.; Tong, W.; Gelovani, J.G. In Vivo 6-([18F]Fluoroacetamido)-1-hexanoic anilide PET Imaging of Altered Histone Deacetylase Activity in Chemotherapy-Induced Neurotoxicity. *Contrast Media Mol. Imaging* **2018**, *2018*, 3612027. [[CrossRef](#)] [[PubMed](#)]
25. Yeh, S.H.; Lin, M.H.; Leo Garcia, F., II; Mukhopadhyay, U.; Young, D.; Ogawa, K.; Jeong, H.J.; Tong, W.; Gelovani, J.G.; Fukumitsu, N. In Vivo Evaluation of the Combined Anticancer Effects of Cisplatin and SAHA in Non-small Cell Lung Carcinoma Using [18F]FAHA and [18F]FDG PET/CT Imaging. *Mol. Imaging* **2021**, *2021*, 6660358. [[CrossRef](#)] [[PubMed](#)]

26. Marks, P.A.; Breslow, R. Dimethyl sulfoxide to vorinostat: Development of this histone deacetylase inhibitor as an anticancer drug. *Nat. Biotechnol.* **2007**, *25*, 84–90. [[CrossRef](#)] [[PubMed](#)]
27. Wang, C.; Schroeder, F.A.; Wey, H.Y.; Borra, R.; Wagner, F.F.; Reis, S.; Kim, S.W.; Holson, E.B.; Haggarty, S.J.; Hooker, J.M. In vivo imaging of histone deacetylases (HDACs) in the central nervous system and major peripheral organs. *J. Med. Chem.* **2014**, *57*, 7999–8009. [[CrossRef](#)]
28. Schroeder, F.A.; Wang, C.; Van de Bittner, G.C.; Neelamegam, R.; Takakura, W.R.; Karunakaran, A.; Wey, H.Y.; Reis, S.A.; Gale, J.; Zhang, Y.L.; et al. PET imaging demonstrates histone deacetylase target engagement and clarifies brain penetrance of known and novel small molecule inhibitors in rat. *ACS Chem. Neurosci.* **2014**, *5*, 1055–1062. [[CrossRef](#)]
29. Wey, H.Y.; Wang, C.; Schroeder, F.A.; Logan, J.; Price, J.C.; Hooker, J.M. Kinetic Analysis and Quantification of [¹¹C]Martinostat for in Vivo HDAC Imaging of the Brain. *ACS Chem. Neurosci.* **2015**, *6*, 708–715. [[CrossRef](#)]
30. Wey, H.Y.; Gilbert, T.M.; Zurcher, N.R.; She, A.; Bhanot, A.; Taillon, B.D.; Schroeder, F.A.; Wang, C.; Haggarty, S.J.; Hooker, J.M. Insights into neuroepigenetics through human histone deacetylase PET imaging. *Sci. Transl. Med.* **2016**, *8*, 351ra106. [[CrossRef](#)]
31. Skipper, P.L.; Tannenbaum, S.R.; Thilly, W.G.; Furth, E.E.; Bishop, W.W. Mutagenicity of Hydroxamic Acids and the Probable Involvement of Carbamoylation. *Cancer Res.* **1980**, *40*, 4704–4708.
32. Subramanian, S.; Bates, S.E.; Wright, J.J.; Espinoza-Delgado, I.; Piekarz, R.L. Clinical Toxicities of Histone Deacetylase Inhibitors. *Pharmaceuticals* **2010**, *3*, 2751–2767. [[CrossRef](#)] [[PubMed](#)]
33. Shen, S.; Kozikowski, A.P. Why Hydroxamates May Not Be the Best Histone Deacetylase Inhibitors—What Some May Have Forgotten or Would Rather Forget? *ChemMedChem* **2016**, *11*, 15–21. [[CrossRef](#)] [[PubMed](#)]
34. Zhang, L.; Zhang, J.; Jiang, Q.; Zhang, L.; Song, W. Zinc binding groups for histone deacetylase inhibitors. *J. Enzyme Inhib. Med. Chem.* **2018**, *33*, 714–721. [[CrossRef](#)]
35. Seo, Y.J.; Kang, Y.; Muench, L.; Reid, A.; Caesar, S.; Jean, L.; Wagner, F.; Holson, E.; Haggarty, S.J.; Weiss, P.; et al. Image-guided synthesis reveals potent blood-brain barrier permeable histone deacetylase inhibitors. *ACS Chem. Neurosci.* **2014**, *5*, 588–596. [[CrossRef](#)] [[PubMed](#)]
36. Hooker, J.M.; Kim, S.W.; Alexoff, D.; Xu, Y.; Shea, C.; Reid, A.; Volkow, N.; Fowler, J.S. Histone deacetylase inhibitor, MS-275, exhibits poor brain penetration: PK studies of [¹¹C]MS-275 using Positron Emission Tomography. *ACS Chem. Neurosci.* **2010**, *1*, 65–73. [[CrossRef](#)]
37. Moradei, O.M.; Mallais, T.C.; Frechette, S.; Paquin, I.; Tessier, P.E.; Leit, S.M.; Fournel, M.; Bonfils, C.; Trachy-Bourget, M.C.; Liu, J.; et al. Novel aminophenyl benzamide-type histone deacetylase inhibitors with enhanced potency and selectivity. *J. Med. Chem.* **2007**, *50*, 5543–5546. [[CrossRef](#)]
38. Methot, J.L.; Chakravarty, P.K.; Chenard, M.; Close, J.; Cruz, J.C.; Dahlberg, W.K.; Fleming, J.; Hamblett, C.L.; Hamill, J.E.; Harrington, P.; et al. Exploration of the internal cavity of histone deacetylase (HDAC) with selective HDAC1/HDAC2 inhibitors (SHI-1:2). *Bioorg. Med. Chem. Lett.* **2008**, *18*, 973–978. [[CrossRef](#)] [[PubMed](#)]
39. Paris, M.; Porcelloni, M.; Binaschi, M.; Fattori, D. Histone deacetylase inhibitors: From bench to clinic. *J. Med. Chem.* **2008**, *51*, 1505–1529. [[CrossRef](#)]
40. Bressi, J.C.; Jennings, A.J.; Skene, R.; Wu, Y.; Melkus, R.; De Jong, R.; O’Connell, S.; Grimshaw, C.E.; Navre, M.; Gangloff, A.R. Exploration of the HDAC2 foot pocket: Synthesis and SAR of substituted N-(2-aminophenyl)benzamides. *Bioorg. Med. Chem. Lett.* **2010**, *20*, 3142–3145. [[CrossRef](#)]
41. Wambua, M.K.; Nalawansa, D.A.; Negmeldin, A.T.; Pflum, M.K. Mutagenesis studies of the 14 Å internal cavity of histone deacetylase 1: Insights toward the acetate-escape hypothesis and selective inhibitor design. *J. Med. Chem.* **2014**, *57*, 642–650. [[CrossRef](#)]
42. Rogers, G.A.; Stone-Elander, S.; Ingvar, M.; Eriksson, L.; Parsons, S.M.; Widén, L. 18F-labelled vesamicol derivatives: Syntheses and preliminary in vivo small animal positron emission tomography evaluation. *Nucl. Med. Biol.* **1994**, *21*, 219–230. [[CrossRef](#)]
43. Sorger, D.; Scheunemann, M.; Grossmann, U.; Fischer, S.; Vercouille, J.; Hiller, A.; Wenzel, B.; Roghani, A.; Schliebs, R.; Brust, P.; et al. A new 18F-labeled fluoroacetylmorpholino derivative of vesamicol for neuroimaging of the vesicular acetylcholine transporter. *Nucl. Med. Biol.* **2008**, *35*, 185–195. [[CrossRef](#)]
44. Hu, K.Z.; Wang, H.; Huang, T.; Tang, G.; Liang, X.; He, S.; Tang, X. Synthesis and biological evaluation of N-(2-[(¹⁸F)fluoropropionyl]-L-methionine for tumor imaging. *Nucl. Med. Biol.* **2013**, *40*, 926–932. [[CrossRef](#)]
45. Hu, K.; Tang, X.; Tang, G.; Yao, S.; Yao, B.; Wang, H.; Nie, D.; Liang, X.; Tang, C.; He, S. 18F-FP-PEG2-beta-Glu-RGD2: A Symmetric Integrin alpha_vbeta₃-Targeting Radiotracer for Tumor PET Imaging. *PLoS ONE* **2015**, *10*, e0138675. [[CrossRef](#)]
46. Tang, C.; Tang, G.; Gao, S.; Liu, S.; Wen, F.; Yao, B.; Nie, D. Radiosynthesis and preliminary biological evaluation of N-(2-[(¹⁸F)fluoropropionyl]-L-glutamine as a PET tracer for tumor imaging. *Oncotarget* **2016**, *7*, 34100–34111. [[CrossRef](#)] [[PubMed](#)]
47. Wang, H.; Zhao, Q.; Dong, W.; Yang, L.; Lu, K.; Guo, X.; Liu, H.; Wei, H.; Cheng, Y.; Wu, Z.; et al. Radiosynthesis and evaluation of N(5)-(2-(¹⁸F-fluoropropanyl) ornithine as a potential agent for tumor PET imaging. *Nucl. Med. Biol.* **2021**, *94–95*, 98–105. [[CrossRef](#)]
48. Demont, E.H.; Bamborough, P.; Chung, C.W.; Craggs, P.D.; Fallon, D.; Gordon, L.J.; Grandi, P.; Hobbs, C.I.; Hussain, J.; Jones, E.J.; et al. 1,3-Dimethyl Benzimidazolones Are Potent, Selective Inhibitors of the BRPF1 Bromodomain. *ACS Med. Chem. Lett.* **2014**, *5*, 1190–1195. [[CrossRef](#)]

49. Methot, J.L.; Hoffman, D.M.; Witter, D.J.; Stanton, M.G.; Harrington, P.; Hamblett, C.; Siliphaivanh, P.; Wilson, K.; Hubbs, J.; Heidebrecht, R.; et al. Delayed and Prolonged Histone Hyperacetylation with a Selective HDAC1/HDAC2 Inhibitor. *ACS Med. Chem. Lett.* **2014**, *5*, 340–345. [[CrossRef](#)]
50. Witter, D.J.; Harrington, P.; Wilson, K.J.; Chenard, M.; Fleming, J.C.; Haines, B.; Kral, A.M.; Secrist, J.P.; Miller, T.A. Optimization of biaryl Selective HDAC1&2 Inhibitors (SHI-1:2). *Bioorg. Med. Chem. Lett.* **2008**, *18*, 726–731. [[CrossRef](#)] [[PubMed](#)]
51. Li, X.; Zhang, Y.; Jiang, Y.; Wu, J.; Inks, E.S.; Chou, C.J.; Gao, S.; Hou, J.; Ding, Q.; Li, J.; et al. Selective HDAC inhibitors with potent oral activity against leukemia and colorectal cancer: Design, structure-activity relationship and anti-tumor activity study. *Eur. J. Chem.* **2017**, *134*, 185–206. [[CrossRef](#)] [[PubMed](#)]
52. Gao, S.; Zang, J.; Gao, Q.; Liang, X.; Ding, Q.; Li, X.; Xu, W.; Chou, C.J.; Zhang, Y. Design, synthesis and anti-tumor activity study of novel histone deacetylase inhibitors containing isatin-based caps and o-phenylenediamine-based zinc binding groups. *Bioorg. Med. Chem.* **2017**, *25*, 2981–2994. [[CrossRef](#)] [[PubMed](#)]
53. La, M.T.; Jeong, B.H.; Kim, H.K. Design and Synthesis of Novel N-(2-aminophenyl)benzamide Derivatives as Histone Deacetylase Inhibitors and Their Antitumor Activity Study. *Bull. Korean Chem. Soc.* **2021**, *42*, 740–743. [[CrossRef](#)]
54. Kilchmann, F.; Marcaida, M.J.; Kotak, S.; Schick, T.; Boss, S.D.; Awale, M.; Gonczy, P.; Reymond, J.L. Discovery of a Selective Aurora A Kinase Inhibitor by Virtual Screening. *J. Med. Chem.* **2016**, *59*, 7188–7211. [[CrossRef](#)]
55. Schäker-Hübner, L.; Haschemi, R.; Büch, T.; Kraft, F.B.; Brumme, B.; Schöler, A.; Jenke, R.; Meiler, J.; Aigner, A.; Bendas, G.; et al. Balancing Histone Deacetylase (HDAC) Inhibition and Drug-likeness: Biological and Physicochemical Evaluation of Class I Selective HDAC Inhibitors. *ChemMedChem* **2022**, e202100755. [[CrossRef](#)] [[PubMed](#)]
56. Bratteby, K.; Shalgunov, V.; Battisti, U.M.; Petersen, I.N.; van den Broek, S.L.; Ohlsson, T.; Gillings, N.; Erlandsson, M.; Herth, M.M. Insights into Elution of Anion Exchange Cartridges: Opening the Path toward Aliphatic (18)F-Radiolabeling of Base-Sensitive Tracers. *ACS Pharmacol. Transl. Sci.* **2021**, *4*, 1556–1566. [[CrossRef](#)] [[PubMed](#)]
57. Cox, D.P.; Terpinski, J.; Lawrynowicz, W. Anhydrous Tetrabutylammonium Fluoride—A Mild but Highly Efficient Source of Nucleophilic Fluoride-Ion. *J. Org. Chem.* **1984**, *49*, 3216–3219. [[CrossRef](#)]
58. Pike, V.W. PET radiotracers: Crossing the blood-brain barrier and surviving metabolism. *Trends Pharmacol. Sci.* **2009**, *30*, 431–440. [[CrossRef](#)] [[PubMed](#)]
59. Van de Waterbeemd, H.; Camenisch, G.; Folkers, G.; Chretien, J.R.; Raevsky, O.A. Estimation of blood-brain barrier crossing of drugs using molecular size and shape, and H-bonding descriptors. *J. Drug Target.* **1998**, *6*, 151–165. [[CrossRef](#)]
60. Waterhouse, R.N. Determination of lipophilicity and its use as a predictor of blood-brain barrier penetration of molecular imaging agents. *Mol. Imaging Biol.* **2003**, *5*, 376–389. [[CrossRef](#)]
61. Lindemann, M.; Moldovan, R.P.; Hinz, S.; Deuther-Conrad, W.; Gundel, D.; Dukic-Stefanovic, S.; Toussaint, M.; Teodoro, R.; Juhl, C.; Steinbach, J.; et al. Development of a Radiofluorinated Adenosine A2B Receptor Antagonist as Potential Ligand for PET Imaging. *Int. J. Mol. Sci.* **2020**, *21*, 3197. [[CrossRef](#)]
62. Seto, E.; Yoshida, M. Erasers of histone acetylation: The histone deacetylase enzymes. *Cold Spring Harb. Perspect. Biol.* **2014**, *6*, a018713. [[CrossRef](#)]
63. Hiranaka, S.; Tega, Y.; Higuchi, K.; Kurosawa, T.; Deguchi, Y.; Arata, M.; Ito, A.; Yoshida, M.; Nagaoka, Y.; Sumiyoshi, T. Design, Synthesis, and Blood-Brain Barrier Transport Study of Ppyriline Derivatives as Histone Deacetylase Inhibitors. *ACS Med. Chem. Lett.* **2018**, *9*, 884–888. [[CrossRef](#)]
64. Yakubovich, A.Y.; Gitel, P.O. Some properties of α -fluoronitriles. *J. Gen. Chem. USSR* **1966**, *36*, 889–891.
65. Banks, J.W.; O'Hagan, D. The enzymatic resolution of an α -fluoroamide by an acylase. *J. Fluor. Chem.* **2000**, *102*, 235–238. [[CrossRef](#)]
66. Rotering, S.; Franke, K.; Zessin, J.; Brust, P.; Fuchtnner, F.; Fischer, S.; Steinbach, J. Convenient recycling and reuse of bombarded [^{18}O]H $_2\text{O}$ for the production and the application of [^{18}F]F $^-$. *Appl. Radiat. Isot.* **2015**, *101*, 44–52. [[CrossRef](#)] [[PubMed](#)]
67. Lindemann, M.; Hinz, S.; Deuther-Conrad, W.; Namasivayam, V.; Dukic-Stefanovic, S.; Teodoro, R.; Toussaint, M.; Kranz, M.; Juhl, C.; Steinbach, J.; et al. Radiosynthesis and in vivo evaluation of a fluorine-18 labeled pyrazine based radioligand for PET imaging of the adenosine A2B receptor. *Bioorg. Med. Chem.* **2018**, *26*, 4650–4663. [[CrossRef](#)] [[PubMed](#)]
68. Schäker-Hübner, L.; Warstat, R.; Ahlert, H.; Mishra, P.; Kraft, F.B.; Schliehe-Diecks, J.; Scholer, A.; Borkhardt, A.; Breit, B.; Bhatia, S.; et al. 4-Acyl Pyrrole Capped HDAC Inhibitors: A New Scaffold for Hybrid Inhibitors of BET Proteins and Histone Deacetylases as Antileukemia Drug Leads. *J. Med. Chem.* **2021**, *64*, 14620–14646. [[CrossRef](#)] [[PubMed](#)]
69. Heltweg, B.; Dequiedt, F.; Verdin, E.; Jung, M. Nonisotopic substrate for assaying both human zinc and NAD $^+$ -dependent histone deacetylases. *Anal. Biochem.* **2003**, *319*, 42–48. [[CrossRef](#)]